Article:
Mehtab, R., Zulkifli, N.W.B.M., Bin Mohd Sabri, M.F. et al. (5 more authors) (2025) Tribological properties of oil palm fiber-derived graphene coatings on piston ring; influence of hydrogen flow rate during CVD process. Wear, 572-573. 206054. ISSN: 0043-1648

https://doi.org/10.1016/j.wear.2025.206054

Tribological Properties of Oil Palm Fiber-Derived Graphene Coatings on Piston Ring; Influence of Hydrogen Flow Rate during CVD process

Raied Mehtab[1], Nurin Wahidah Binti Mohd Zulkifli[1]*, Mohd Faizul Bin Mohd Sabri[1], Ardian Morina[2], Mohd Fadzli Bin Abdollah[3], Hilmi Bin Amiruddin[3], Syahrullail Bin Samion[4], Mohamad Firdaus bin Saharudin[1]

[1] Department of Mechanical Engineering, Faculty of Engineering, Universiti of Malaya, Malaysia

[2] School of Mechanical Engineering, University of Leeds, UK

[3] Faculty of Mechanical Technology and Engineering, Universiti Teknikal Malaysia, Malaysia

[4] Faculty of Mechanical Engineering, Universiti Teknologi Malaysia, Malaysia

Corresponding author nurinmz@um.edu.my*

Abstract

This study aims to investigate the influence of varying hydrogen flow rates on the tribological properties of graphene-coated piston rings developed via chemical vapor deposition (CVD) with oil palm fiber as precursor. Graphene was derived from oil palm fiber and polystyrene with varying Hydrogen (H_2) flow rate in the CVD process i.e, 200, 400, 600 and 800 sccm and deposited on piston rings. The tribological tests were conducted using a high-frequency reciprocating rig (HFRR) according to ASTM G181 – 11 engineering standards. The load of 10N was kept constant for each test and the test was performed till 300m sliding distance was attained. Among all four hydrogen flow rates, it was observed that graphene-coated piston ring developed with 600 sccm and 800 sccm hydrogen flow rates show enhanced tribological properties when derived from 100 wt% of oil palm fiber and polystyrene respectively. The coated piston ring results were compared with non-coated commercially used piston rings and it was found that the coefficient of friction and wear rate of 600 sccm oil palm fiber based graphene coated piston ring was reduced by 20% and 70% respectively as compared to uncoated piston ring.

Keywords: Tribology, Graphene coating, Piston ring, Chemical vapor Deposition, Bio-based

1. Introduction:

The quest to improve materials and enhance their properties is driven by the desire to obtain the most efficient, economical and sustainable solutions. Studies have shown that approximately 23% of world's energy consumption is due to wear and friction in machine parts [1]. In a typical fired engine, mechanical friction consumes approximately 4% to 15% of the total fuel energy. Friction losses are predominantly concentrated in three components: the piston-ring-liner interface, the crankshaft, the valvetrain mechanism and the bearing assembly [2]. Among which the friction loss in piston ring reaches up to 26% of total friction losses[3].

[3]In an IC engine, there are usually three piston rings, all having their own functionality. Sealing of the combustion chamber is done by the gas ring, the second is the compression ring and the sweeping of excess oil from the inner surface of the cylinder liner is done by the scraper ring [4]. Among the key characteristics of piston rings sealing combustion gases within the cylinder chamber is important as it restricts the mixing of engine oil with the fuel thus contributing directly towards carbon dioxide emissions. However, piston rings operate under harsh conditions due to high thermal loads from the combustion gases. To ensure durability and reliability, the material of the piston ring must have good sealing properties, high-temperature resistance, wear resistance and a low friction coefficient [5].

As a result, minimizing wear and controlling friction are critical for conservation of energy and protection of the environment, and to achieve this objective, significant efforts have been devoted to developing new materials and technologies [6–8]. One of the primary challenges of minimizing wear and tear is the development of internal combustion engines, while taking into account their greenhouse gas emissions, oil depletion, and environmental pollution [9]. This leads the researchers towards finding a better material for engine components. Numerous properties of a material are checked and the one with the most desirable properties is selected. Mostly the material chosen matches the desired criteria for the selected application, but at times there are some properties that the chosen material does not possess [10].

To overcome this problem, a lot of work has been carried out to enhance the properties of the material, such as alloying, surface coatings, heat treatment etc. Amongst these techniques, the development of surface coatings has contributed more towards surface property enhancement like wear resistance, adhesion, corrosion resistance, hardness, etc.[11]. The coating techniques are most cost effective, and they consume less material as thickness of coatings vary from nanometers to micrometers [12]. Due to virtue of coating techniques, self-lubricating coatings

63 can be utilized to reduce friction and wear, such coatings are developed by incorporating solid
64 lubricants to the base matrix, and possess excellent mechanical, physical, and tribological
65 properties, hence reducing the friction which leads to reduction of temperature on the contacted
66 surface thereby, reducing the thermal loads for the surfaces [13].

67 Solid lubricants are the most promising option in complicated zones where liquid lubrication
68 is not feasible, such as extreme temperature applications and vacuum [14]. In the review of
69 self-lubricating coating or materials, usually following categories of compounds are
70 considered: polymer composite, layered materials such as Graphene, hBN etc, oxides like
71 TiO2, PbO, etc, soft metals [15–18]. Amongst these solid lubricants, graphene is known for
72 being strong material even if it is the thinnest material known, this is due to its strong carbon
73 bonds [19]. Hence making it best suitable for piston ring application. Graphene research is
74 comparatively a new field which has been showing a rapid growth after its first successful
75 exfoliation, back in 2004 by prof Kostya Novoselov and Prof Andre Geim, from a bulk graphite
76 at the university of Manchester [20]. Graphene has shown the most remarkable properties
77 among other sp2 allotropes of carbon.

78 In terms of tribology, It has proved through simulations by Xu et al. that the frictional force
79 significantly gets reduced in few-layer graphene, as the number of layers decrease, eventually
80 reaching zero when only two or three layers remain [21]. Mat Tahir et al. recorded a coefficient
81 of friction (COF) less than 0.15 for graphene coating synthesized via chemical vapor deposition
82 (CVD) method [22]. Graphene has also proved to reduce wear and friction if added as an
83 additive in lubricating oil and has been called as green lubricant additive [23–25].

84 Some researchers used Direct Chemical Vapor Deposition (CVD) technique to synthesize solid
85 lubricant like graphene coating on engine piston rings [26]. There results proved that the
86 graphene coating on piston rings via CVD method has significantly reduced the coefficient of
87 friction compared to uncoated piston rings. Another study found that applying graphene
88 directly as coating even with only few layers significantly enhanced the surface durability
89 under dry sliding conditions. The graphene exhibited consistently lower COF at ambient
90 conditions, mainting stability over thousands of sliding cycles[27].
91
92 Beyond graphene coatings, several other coating techniques have been investigated to improve
93 tribological performance of piston rings. Thermal spray coatings, such as High velocity oxygen
94 flow (HVOF) and plasma spraying have been used lately. HVOF sprayed molybdenum (Mo)

coatings have recorded that wear loss is mostly impacted by load and primarily through abrasion [28,29]. Other comparative studies on Cr-Al2o3, CrN and Mo coatings revealed that CrN coated rings had lower wear depth but slighty higher COF [30].

Researchers have been synthesizing graphene layers using various methods, including Chemical vapor deposition (CVD) technique [31–35]. Mostly during CVD process, the type of precursor of carbon used is CH_4 [36–38]. Nevertheless the reliance of CVD on gaseous precursor is considered as its major limitation. Recently, bio-based carbon precursors are being used for growth of graphene. Salifairus et al. synthesized graphene on nickel sheet from palm oil through CVD technique and recorded that the graphene deposition showed excellent characteristics [39]. The flexibility of CVD coating technique allows researchers to explore and use various carbon precursors, including solid, liquid and gaseous materials. Graphene layers are developed on the surface of substrate by heating the carbon source to its gas transient point, and with the help of inert gases like, hydrogen or argon, the resulting carbon vapor is deposited onto the substrate surface [39–43]. It is due to this versatility of carbon precursors, that research area on CVD synthesized graphene has expanded. However there are limited studies on the use of oil palm fiber (a local waste) as carbon precursor for graphene synthesis and its tribological properties are yet to be explored.

The aim of this research is to develop a graphene coating on piston ring via CVD method from oil palm fiber and polystyrene as carbon precursors and investigate their tribological properties with varying hydrogen flow rates.

2. Experimental Procedure

2.1 Materials

The list of materials used for the tests is given in Table 1. Stainless steel (SS304) samples of dimensions 15mm X 15mm were used as piston ring Counterbody for the tribological tests. Polystyrene was used as one of the carbon precursors to derive graphene via the Chemical Vapor deposition technique.

Table 1: Material procurement details

S No.	Name	Specifications	Seller/Brand
1.	Oil Palm Fiber	Dried Mesocarp fibers	Malaysian Palm Oil Berhad, Malaysia.

2.	Piston Rings	Diameter: 60mm	RIKEN, Riken Corporation, Japan.
3.	Motor Oil	0W-20 Shell helix eco fully synthetic	Anglo Oriental Traders Sdn Berhad, Malaysia.

2.2 Methodology

2.2.1 Piston ring preparation

Prior to coating deposition, piston rings were polished with sandpaper to remove the existing coating and maintain the roughness of the piston ring surface to achieve mechanical anchoring of the coating to the substrate. Piston rings were then washed with acetone in an ultrasonic bath for 5 minutes and left dried. This was done to remove the impurities on piston ring and ensure no oxide layer is present. Furthermore, hydrogen that is used in synthesis process also played an important role in removing the oxide layer on the piston ring surface. The chemical reaction involved in this process is given as:

$$Fe_2O_3 + 3H_2 \rightarrow 2Fe + 3H_2O$$

2.2.2 Coating Development

The development of coating has been depicted in Fig. 1. The synthesis process of coated samples was done using Chemical vapor deposition (CVD) process with parameters given in Table 2. The CVD chamber at furnace 2 was used for annealing the clean piston ring for 30 minutes at a heating rate of 60°C/min and with varying range of hydrogen flow rates from 200 to 800 sccm. Hydrogen was used during the annealing process due to its property of eliminating

the oxide layer from the metal surface.

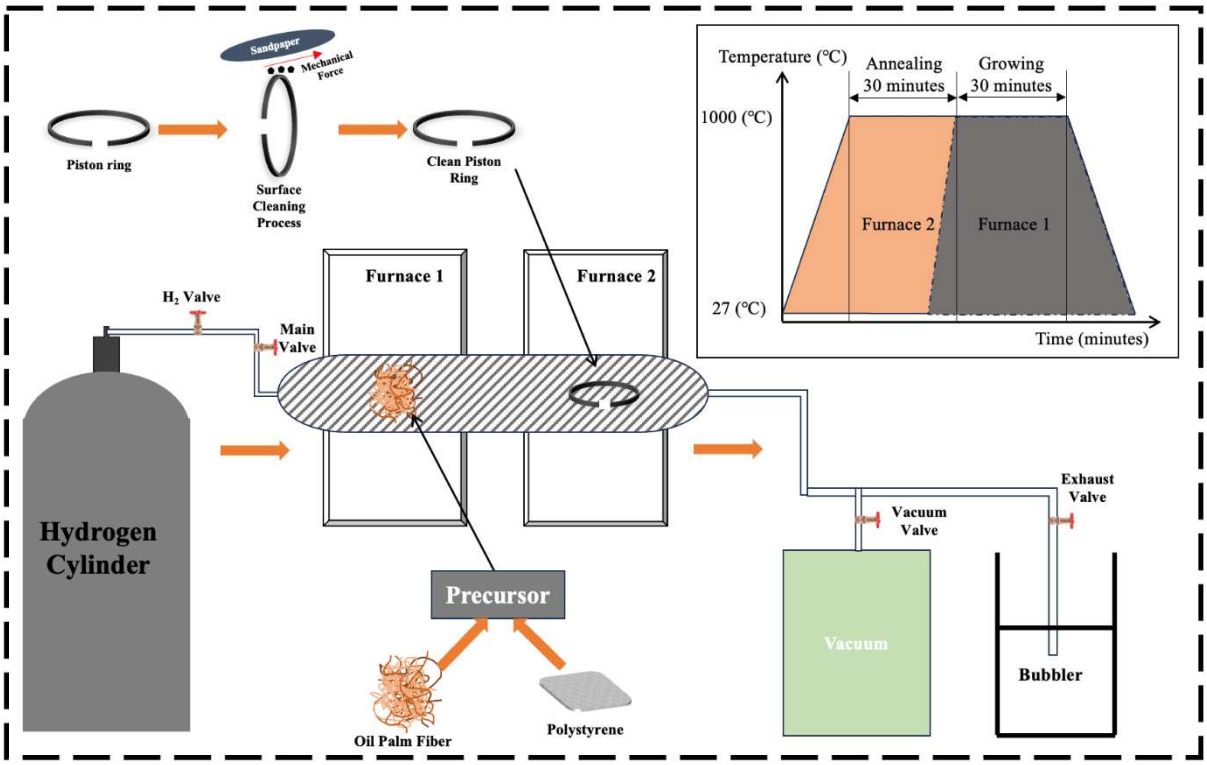

Fig. 1: Schematic Diagram of Chemical Vapor Deposition Process.

Table 2. CVD Process parameter

Furnace 2	Furnace 1
• Piston ring • Annealing temperature: 1020 degree Celsius • Time duration 30 mins • Heating rate: 60 C • Varying Hydrogen flow rate (200-800)	• Carbon precursor • Heated at 1000 Degree Celsius • Under atmospheric pressure • Continuous hydrogen flow • Growth time 30 mins • System was cooled at 80 C/min cooling rate.

As a result, it is crucial for cleaning and crystalizing metal substrates. Moreover, molecular hydrogen plays an important role in the development of graphene on substrate surface, therefore, varying the hydrogen flow rate in CVD process would impact the quality of graphene coating. The system was cooled after the annealing process at furnace 2 and the carbon precursor material; Oil Palm Fiber (OPF)/Polystyrene (PS), was heated in furnace 1 to 1000°C to generate graphene with a continuous hydrogen flow rate at atmospheric pressure. Later the

system was cooled with a cooling rate of 80°C/min. The total growth time was 30 minutes. The nomenclature of piston ring samples according to the hydrogen flow rate and precursor used for their development is given by Table 3.

Table 3. Sample Compositions

Sample	**H_2 Flow [sccm]**	**Precursor**
200 OPF	200	100 wt.% OPF
200 PS	200	100 wt.% PS
400 OPF	400	100 wt.% OPF
400 PS	400	100 wt.% PS
600 OPF	600	100 wt.% OPF
600 PS	600	100 wt.% PS
800 OPF	800	100 wt.% OPF
800 PS	800	100 wt.% PS
PR	Uncoated piston ring	-

2.2.3 Tribological Evaluation

High Frequency Reciprocating rig (HFRR) from DuCom, tribometer was used to investigate tribological properties of the graphene-coated piston rings. The test parameters under which the test was performed are mentioned in Table 4.

Table 4: High frequency reciprocating rig tribometer test parameters.

Parameter	**Value**
Load [N] and Contact Pressure (MPa)	10 (1.25 MPa), 20(2.5 MPa), 30(3.75 MPa) and 40 N (5 MPa)
Stroke length [mm]	8
Time duration [minutes]	30
Sliding Distance	300 m

Estimating and developing a statistical correlation between engine performance parameters and the tribological characteristics of engine components in actual running conditions is quite challenging due to high costs associated with engine modifications. To simplify this process,

tribological characteristics of engine components like piston ring-liner configuration are evaluated using HFRR tribometer [44–47]. The actual gas pressure in an engine is about 4.5 MPa for a heavy duty diesel engine [28,29]. The contact pressure from the arrangement shown in Fig. 2 varies from 1.25 MPa to 5 MPa, thus covering the range for an engine running under low and extreme conditions.

The design of reciprocating rig was modified and developed according to the dimensions of the piston ring as shown in Fig. 2. The HFRR test was conducted as per ASTM 181-11 standards at room temperature, under boundary lubrication conditions using 0W-20 (shell helix eco-fully synthetic motor oil), about 15 ml, with a frequency of 10 Hz. Stainless steel specimens (15 x 15 x 4 mm) were used as counter bodies for the tests. Before each test the stainless-steel (counter body) specimens were polished with 80, 150, 400 and 800 grade sandpaper followed by spraying the polycrystalline dia suspension (5 µm) to get the mirror like finish. All this was done to reduce the impact of roughness of counter body surface on wear and friction test and mimic the actual sliding contact between piston ring and cylinder liner in the piston cylinder assembly.

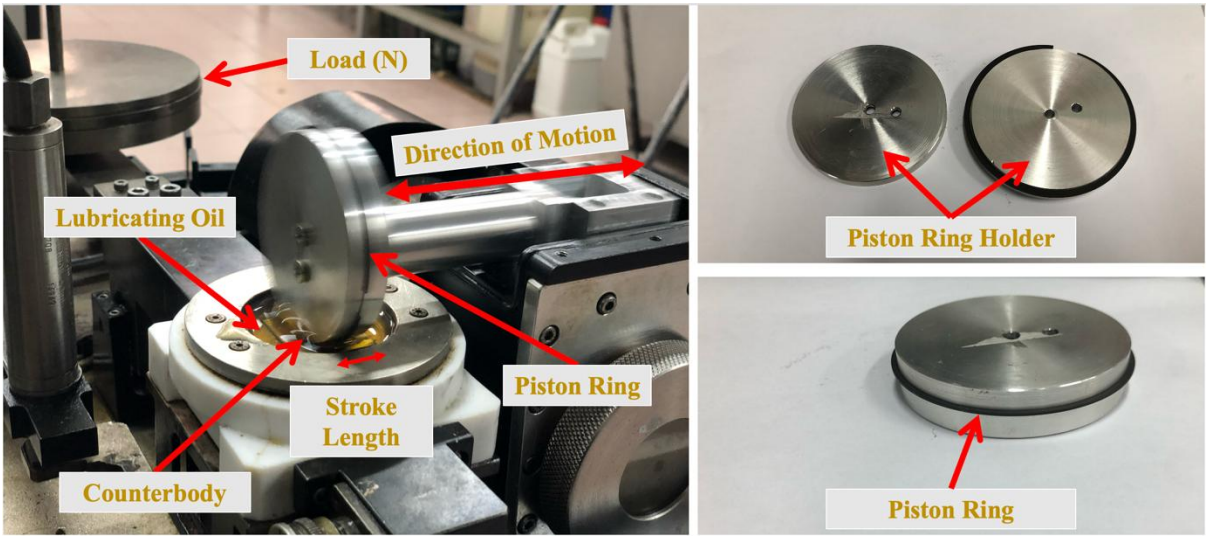

Fig. 2: Piston ring configuration on High Frequency Reciprocating Rig (HFRR) Tribometer

Each Tribological test was conducted three times under the same conditions to ensure repeatability and reduce the experimental variability.

2.2.4 Surface Morphology Analysis

Scanning electron microscopy (SEM, PHENOM-XL Desktop) was used with the combination of Energy dispersive X-ray (EDS) to check the surface morphology of the samples. The wear behaviour of the surface piston ring samples and counterbodies was also done by SEM/EDS. Secondary ion mass spectroscopy (SIMS, HIDEN-Compact SIMS) was used to determine the concentration of graphene oxides on the counterbody surface. BRUKER 3D-Optical

Microscopy based on white light interferometry was used to examine the wear scar profile and to determine the wear rate of counter bodies by calculating volume loss. Raman Spectroscopy was done using RENISHAW-inVia Raman Microscope, to confirm the presence of graphene on coated samples. I_D/I_G values were calculated based on Raman spectroscopy result, to check the quality of graphene coating.

3. Results and discussions:

3.1 Surface Morphology

The surface morphology of the coated surface of piston ring is analysed using SEM. Fig. 3 (a, b) shows the SEM images at 2000x magnification for samples 600 OPF and 800 OPF respectively.

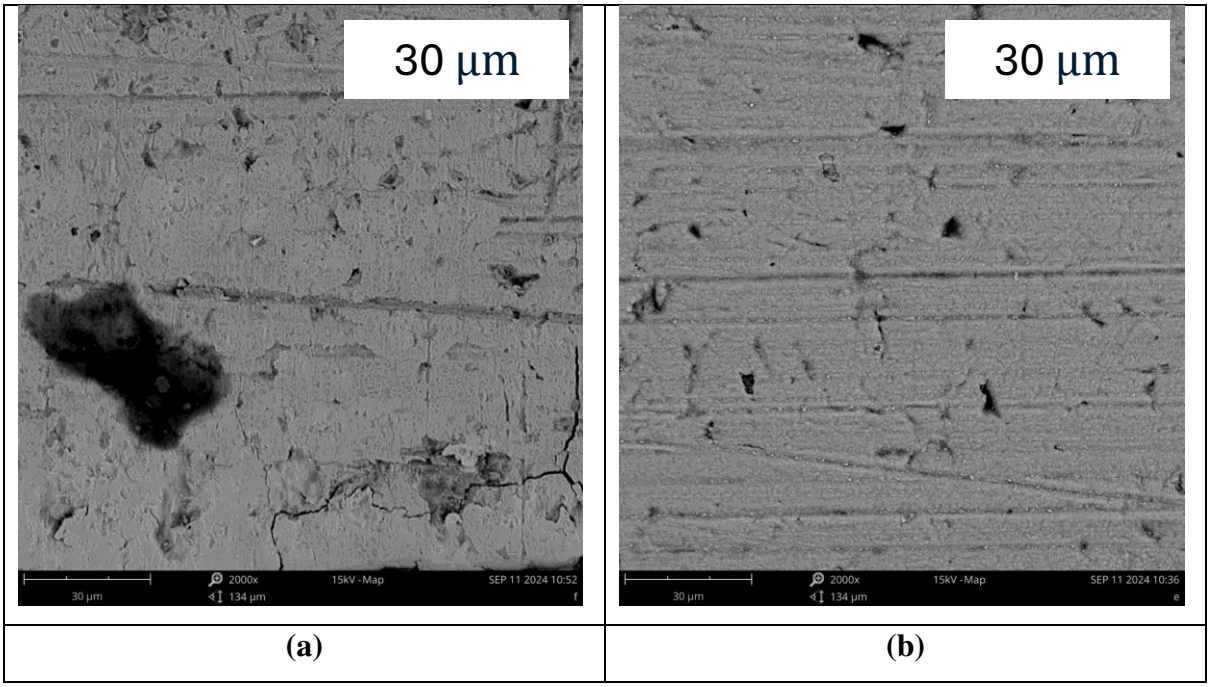

(a) **(b)**

Fig. 3: SEM Images of (a) 600 OPF and (b) 800 OPF coated surfaces.

For 600 OPF specimen, Fig. 3 a, the surface appears relatively smooth with a fine, uniform distribution of the graphene coating. There are few observable microstructural irregularities, including small defects and minor cracks. However, the overall surface exhibits a relatively consistent and compact structure with minimal porosity. Some dark region in the image depict the agglomerations of graphene flakes.

In contrast, 800 OPF sample, Fig. 3 b, shows a noticeable rougher surface morphology with visible cracks and microvoids. The presence of larger defects and irregularities may be attributed to higher hydrogen flow rates during CVD process potentially leading to increased etching effects or non-uniform deposition.

The cross sectional analysis of coated and non-coated piston rings have been conducted using energy dispersive X-ray spectroscopy and scanning electron microscopy in order to confirm the presence of coating layer and to determine the thickness of coating layer on substrate. Fig. 4 shows the SEM-EDX mapping of cross section of 600 OPF coated piston ring.

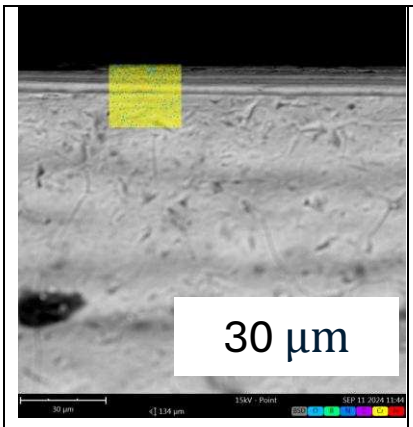

Element Number	Element Symbol	Element Name	Atomic Conc.	Weight Conc.
8	O	Oxygen	29.90	32.80
5	B	Boron	29.64	21.96
7	N	Nitrogen	18.85	18.10
6	C	Carbon	18.20	14.98
24	Cr	Chromium	3.38	12.04
26	Fe	Iron	0.03	0.12

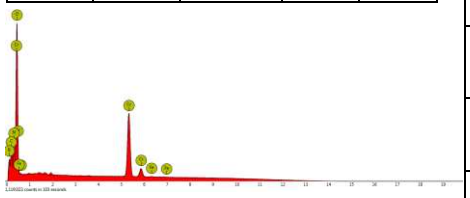

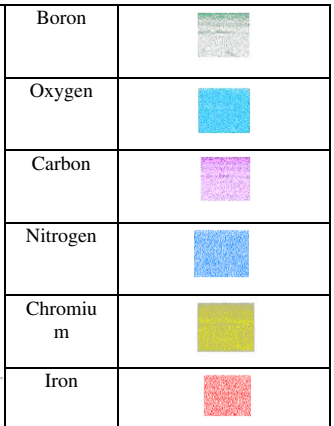

(a) (b) (c)

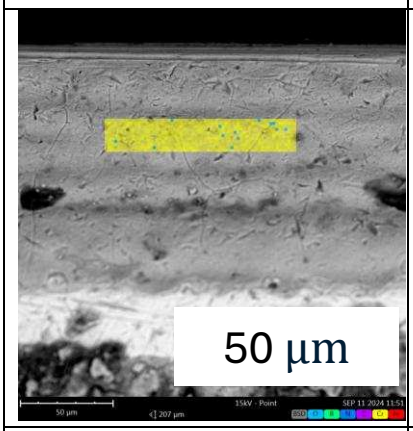

Element Number	Element Symbol	Element Name	Atomic Conc.	Weight Conc.
8	O	Oxygen	35.57	35.99
5	B	Boron	22.88	15.64
7	N	Nitrogen	20.45	18.11
6	C	Carbon	15.47	11.75
24	Cr	Chromium	5.54	18.20
26	Fe	Iron	0.09	0.31

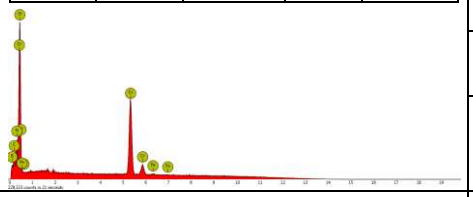

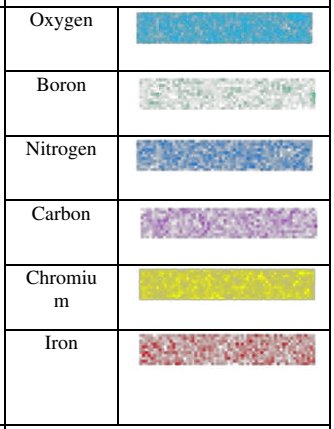

(d) (e) (f)

Fig. 4: (a) SEM and EDX mapping showing the coated layer, (b) Elemental analysis of coated layer, (c) Elemental distribution based on colour coding of coated layer, (d) SEM-EDX Mapping showing the substrate, (e) Elemental analysis of the substrate, (f) Elemental distribution based on colour coding of the substrate, coated piston ring – 600 OPF

It is observed from Fig. 4 that the graphene coating is successfully deposited over the substrate, with increase in carbon element atomic and weight concentration. Also it can be clearly seen that the carbon is evenly distributed depicting even distribution of graphene layers. Fig. 5 shows the cross sectional SEM image of non coated and coated samples. It can be observed from Fig. 5 that the average thickness of graphene coating is around 10µm±1. While as the thickness of chromium on non-graphene coated piston ring is around 200µm±20.

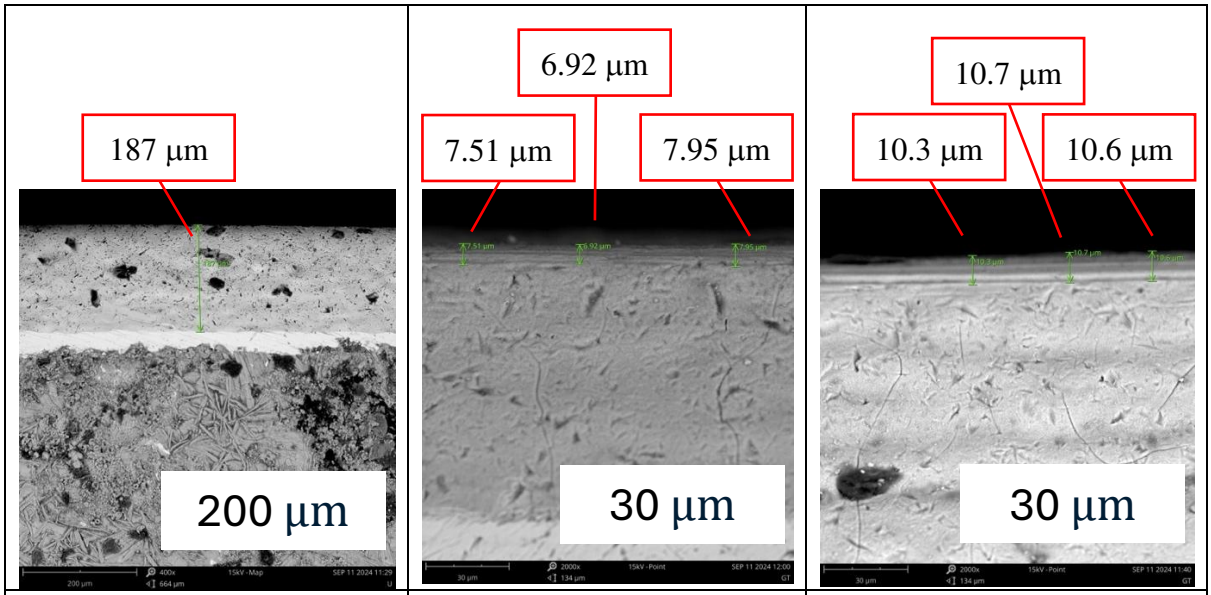

(a) Uncoated piston ring (b) 600 OPF (c) 600 OPF

Fig. 5: (a) SEM image of cross section of non-graphene coated piston ring, (b, c) SEM image of cross section of 600 OPF graphene coated piston ring.

3.2 Coefficient of friction

The friction behaviour of all graphene coated piston rings and non-graphene coated piston ring against stainless steel counter body at load 10N is shown in Fig. 6.

It is observed from the friction curves that initially the COF fluctuated and reached its maximum point and gradually came down after some time. After sometime almost for all curves, except 800 OPF and 600 PS which is discussed in effect of hydrogen flow rate below, it can be clearly seen that the samples adapted to the testing conditions and showed steady state thereafter. This could be attributed to the formation of true contact area within contacting surfaces. The variation in COF of all graphene coating compositions ranged between 0.1 to 0.15. Overall COF reduction was observed in graphene coated piston rings as compared to non-graphene coated piston rings. The reduction in the COF due to graphene coating has also been reported by other researchers in their work [22].

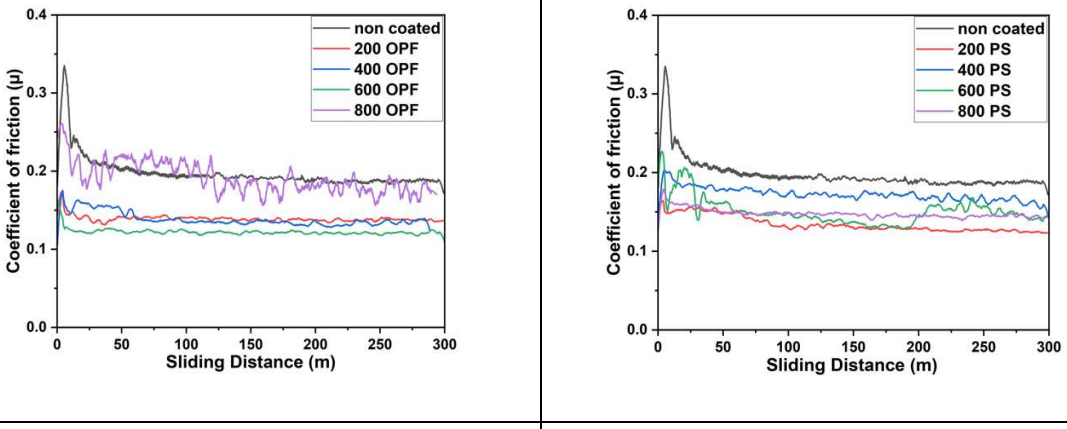

(a) (b)

Fig. 6: COF curve of (a) OPF & (b) PS coated samples under load 10 N

Amongst all tested samples subjected to load 10 N, it is observed that the piston ring coated with 600 OPF graphene exhibited the lowest COF and the COF variation with respect to sliding distance is very less.

3.2.1 Effect of carbon precursors on friction

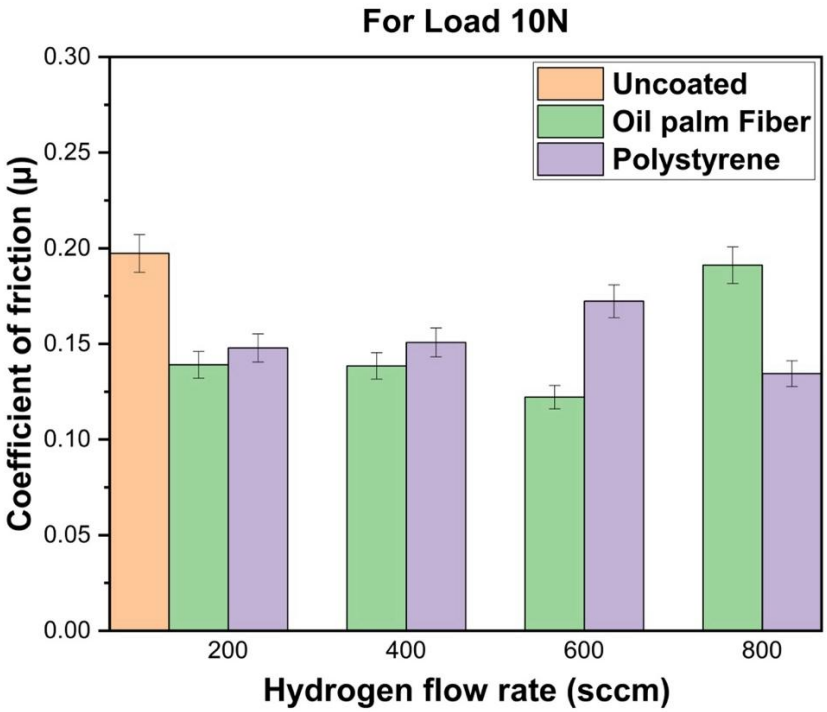

Fig. 7: Average COF of all samples under load 10N

Fig. 7 shows the overall average coefficient of friction (COF) of the non-graphene coated piston ring, Oil palm fiber (OPF) based graphene coated piston rings and the polystyrene based graphene coated piston rings for load 10 N. The error bars in the graph represent the standard deviation (SD) of the COF values obtained from three repeated tests. Larger error bars observed

in certain condition (600 PS at 200m and 800 OPF) suggest variations in tribological behaviour, which may be due to coating adhesion or wear debris accumulation.

It can be observed that the average coefficient of friction for oil palm fiber-based graphene coated piston rings have shown least values of COF compared to polystyrene-based graphene coated piston ring and non-graphene coated piston ring. The superiority of COF result for oil palm fiber-based graphene coated piston rings could be attributed to the excellent quality of graphene coating that are produced by this carbon precursor [39]. Furthermore, the reason behind this is discussed in detail below.

3.2.2 Effect of hydrogen flow rate on friction

The results shown in Fig. 7 depict that with increase in hydrogen flow rate within oil palm fiber-based graphene coated piston ring samples, the COF has decreased, with minimum value for 600 OPF 0.13±0.001 and increased for 800 OPF and 600 PS.

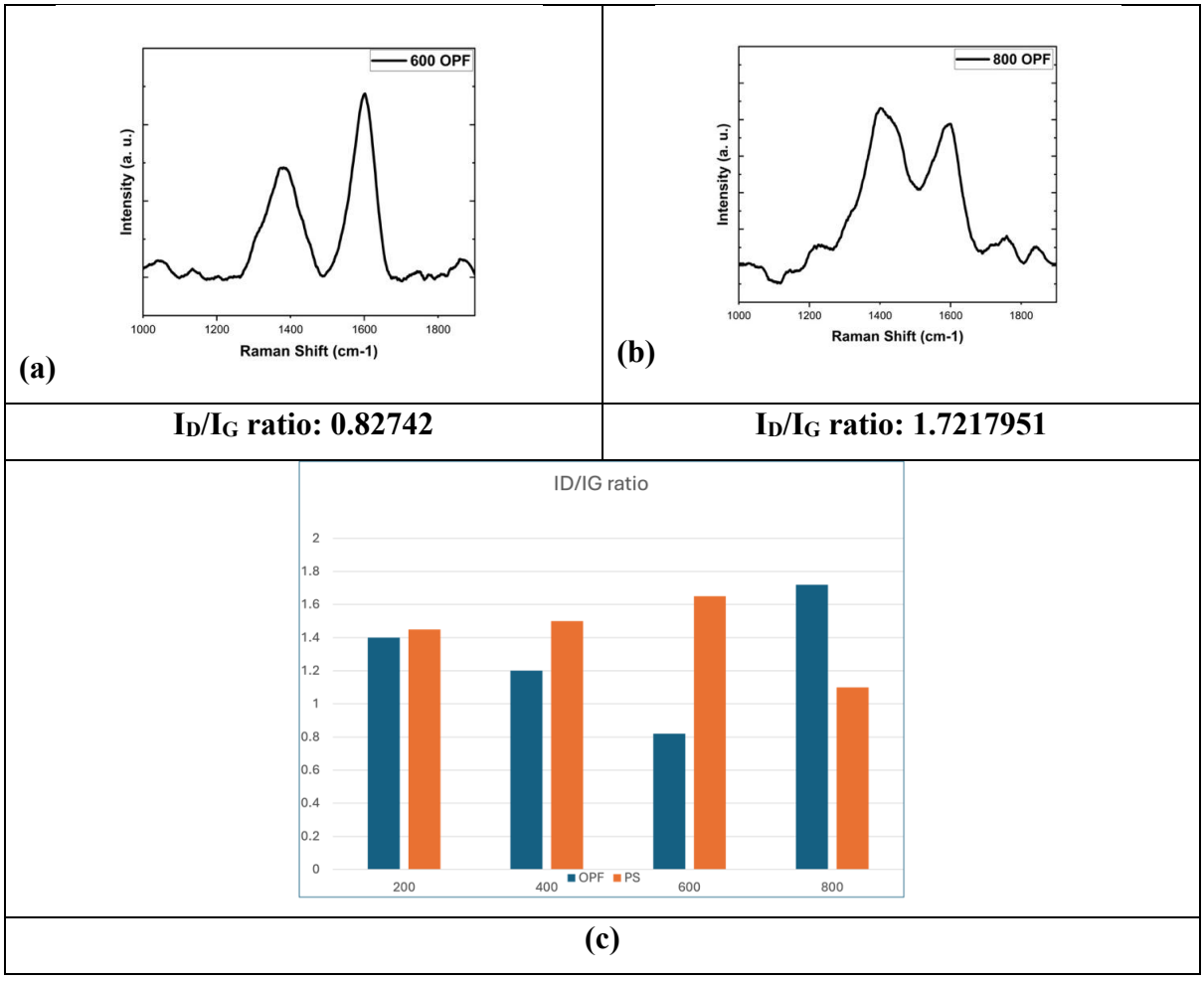

Fig. 8: Raman Spectroscopy of (a) 600 OPF and (b) 800 OPF piston rings and (c) Raman Spectroscopy graph for all samples

To further clarify the reason behind this, Raman spectroscopy was conducted for OPF samples with varying hydrogen flow rate. Fig. 8 represents the Raman Spectroscopy results. The peaks in Fig. 8 (a, b) depict the presence of graphene in oxide forms, as for graphene oxide (GO), the D peak usually appears around 1350-1360 cm-1, and G peak around 1580-1600 cm-1[22,48]. GO is hydrophilic while as pure graphene is hydrophobic, which adds to the advantage of this study as GO is best suitable for lubricated test conditions. Fig. 8 (c) shows the ID/IG ratio of Raman spectroscopy of these samples. It can be seen that for 600 OPF that the ratio of intensity of defects to intensity of graphitic or sp2 carbon bonds is less compared to 800 OPF, confirming that the quality of graphene layer synthesised by OPF carbon precursor at 600 hydrogen flow rate is superior. Whereas for Polystyrene (PS) precursor, the ratio is highest for 600 hydrogen flowrate, depicting the quality of graphene being less relatively. The sudden increase in COF for sample 600 PS at 200m Sliding distance can be attributed to the quality of graphene coating, compromising its adhesion to the surface which may have led to peeling of the coating while tribological test.

Considering the results from Raman and COF, it was concluded that 600 OPF-based graphene coating is optimum for our application. Further tests were carried for 600 OPF-based graphene coated piston ring in order to determine the effect of varying loads from 10 N to 40 N.

3.2.3 Effect of load on friction

Fig. 9 shows the average COF graph of 600 OPF samples with varying loads. It is depicted that COF of 600 OPF coated piston rings increase with the increase in load till 30 N and therafter it decreases. The rise in the friction coefficient is attributed to the deep penetration of the hard aperities under increased loads, which inturn led to adhesion and ploghing. The decrease of COF from 30N to 40N is attributed to the removal of some graphene oxide layers from the coated piston ring and formation of graphene oxide layer on Counterbody due to high load. Increase of graphene oxide layers on counterody surface enhances the tribo characteristic of the sliding contact hence reducing the frictional force. To confirm the presence and concentration of GO on the counterbodies, secondary ion mass spectrometry (SIMS) was used and the results are shown by Fig. 10.

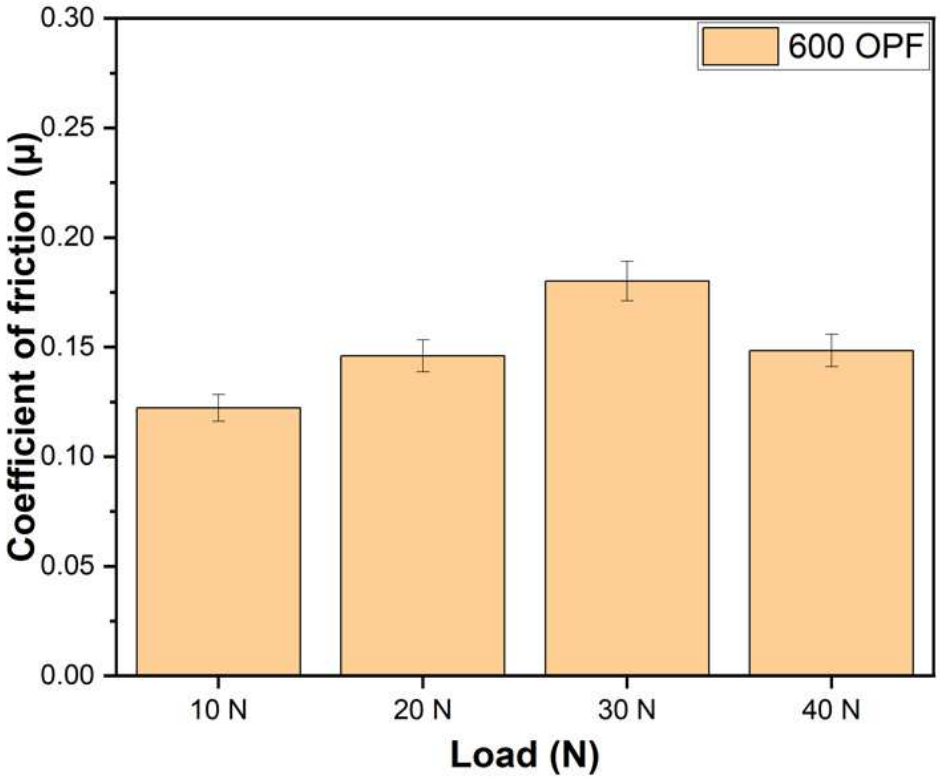

Fig. 9: COF graph of sample 600 OPF piston ring under varying loads

From Fig. 10, it was observed that the compound with 27 amu had increased on the Counterbody with increase in load till 30 N and got decreased for load 40 N. As we know, atomic mass of graphene (carbon) is 12-14 amu and also for oxygen, it is 16 amu. It can be concluded that the peak at 27 amu in the results of SIMS is of graphene oxide. At 40 N the concentration of GO decreased from the intensity of GO at 30 N, hence COF reduction could be due to decrease in layer of graphene coating, as it was recorded in past literature also, that graphene with decreasing layer or thickness shows drastic reduction in COF [21].

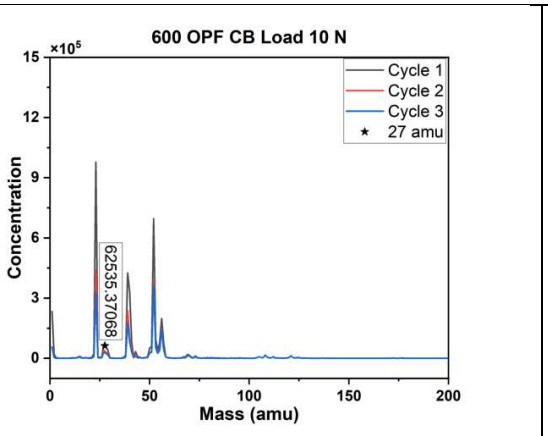

(a)

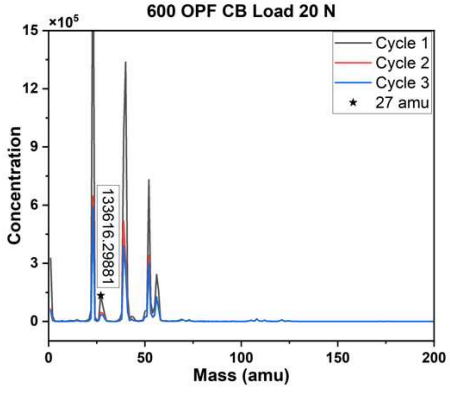

(b)

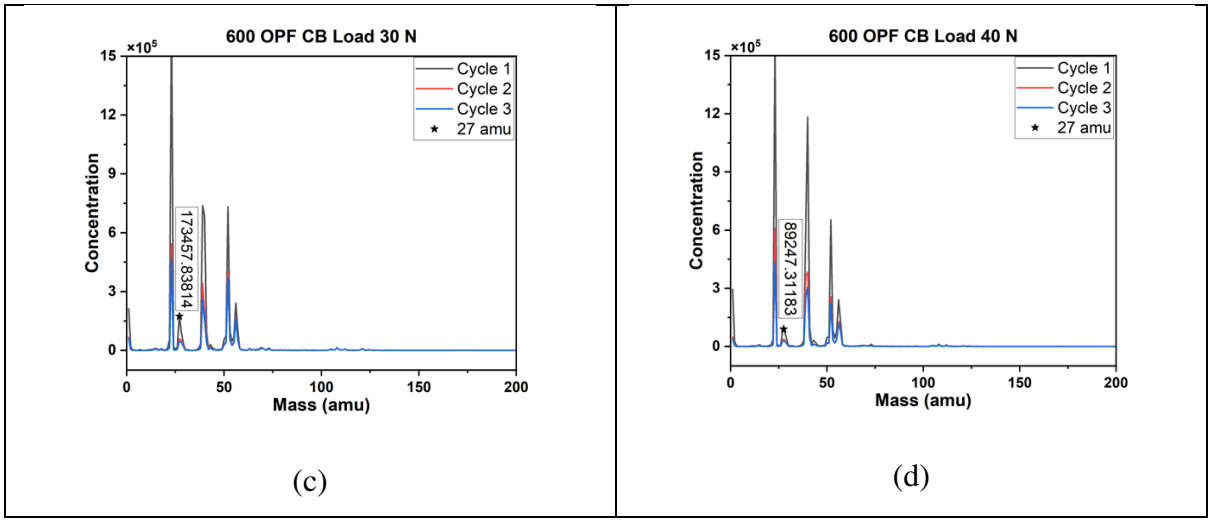

Fig. 10: SIMS graph of counterbody subjected to load (a) 10N, (b) 20 N, (c) 30 N and (d) 40N.

To understand further, Raman spectroscopy of 600 OPF-based graphene coated piston rings subjected to tribological test was conducted. The Raman spectroscopy graph is given by Fig.11, where the intensity of GO is observed to be much more in coated piston ring at 40 N than the samples subjected to loads 30, 20 and 10 N.

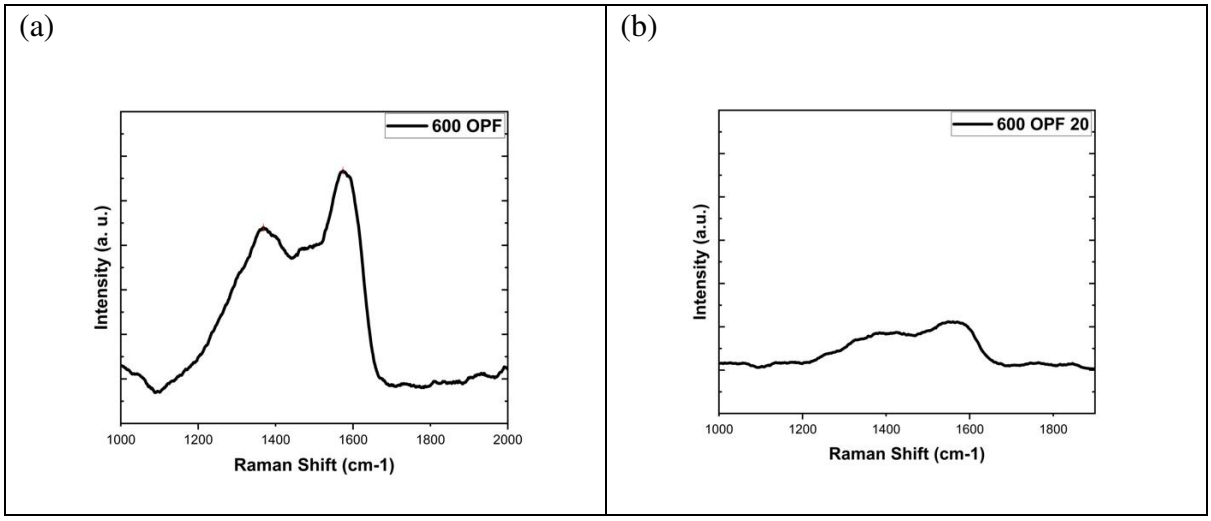

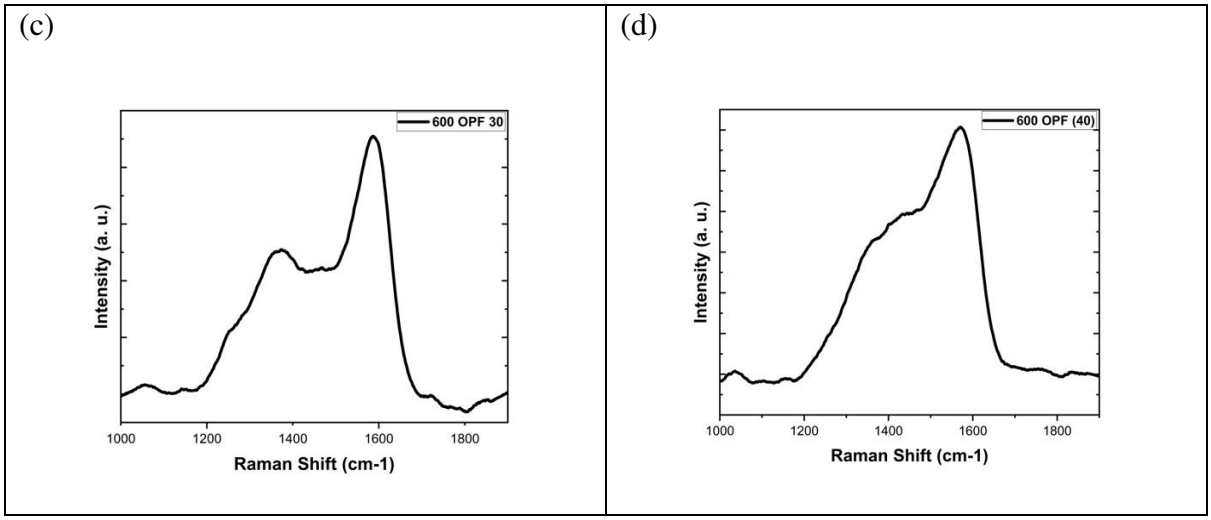

316 Fig. 11: Raman Spectroscopy graphs of sample 600 OPF piston ring at load (a) 10N, (b) 20
317 N, (c) 30 N and (d) 40N

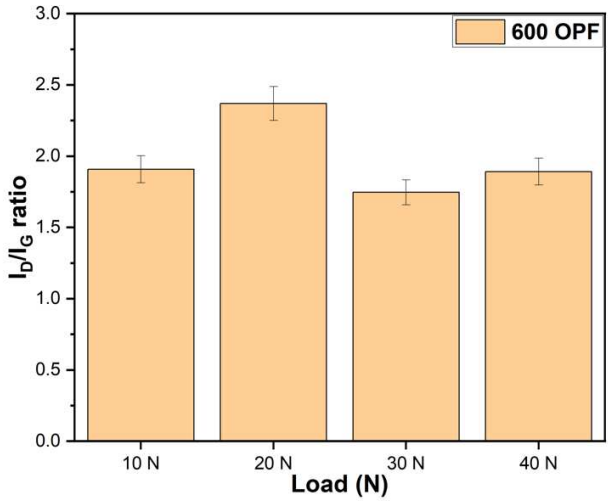

318 .

319 Fig. 12: ID/IG ratio graph for sample 600 OPF piston ring under varying loads

320 Fig. 12 shows the ratio of the intensity of defects to the intensity of Graphitic or carbon sp2
321 bonds for the Raman spectroscopy graphs shown in Fig. 11. It is observed from Fig. 12 that the
322 quality of 600 OPF coating on piston post tribological test for load 20N, was reduced and ID/IG
323 ratio was increased.

324 Overall, the CVD graphene coated piston rings showed significant reduction in Coefficient of
325 friction values compared to past literature[49]. Fig. 13 shows the comparison between the
326 average COF values of commercially coated piston rings with the present work.

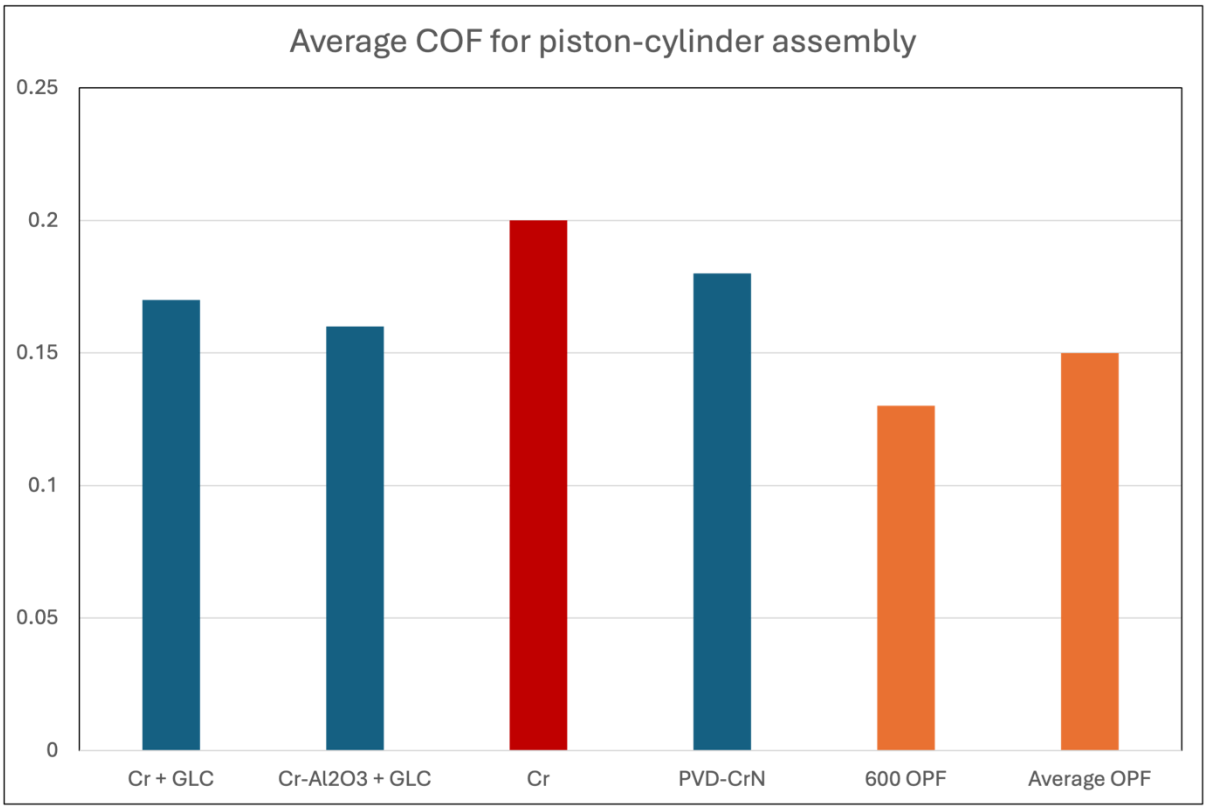

Fig. 13: Comparison of COF of piston ring application

3.3 Wear behaviour

3.3.1 Wear rate

The wear rate of samples is calculated by dividing the volume lost by the sliding distance [50].

$$\text{Wear rate} = \text{Volume lost} \div \text{Sliding Distance}$$

The volume lost was calculated by subtracting the weight of piston ring after the tribological test from the weight of piston ring sample before the test. Before weight recording each sample was ultrasonically cleaned, to ensure minimum wear debris on the sample surface.

The wear rate of the samples against load 10N is shown below in Fig. 14. It is recorded that the wear rate of non-graphene coated piston ring is relatively higher than that of graphene coated piston ring the samples overall. Graphene coating synthesized via CVD has significantly reduced the wear rate by more than 60% in piston rings at load 10 N.

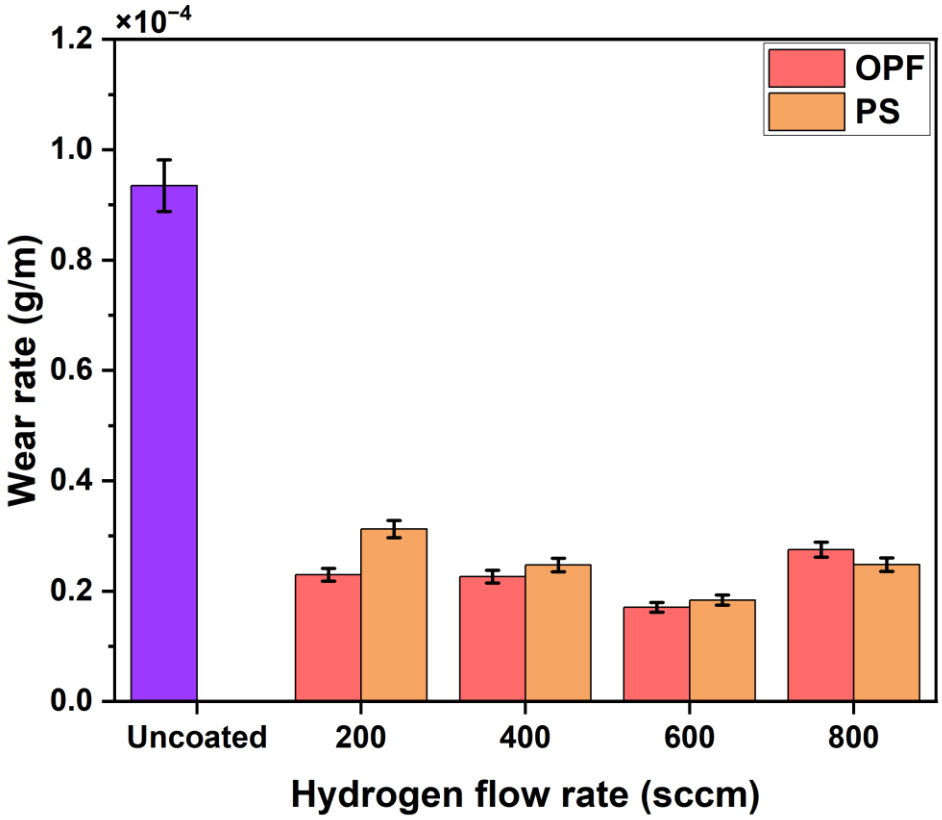

Fig. 14: Wear rate of piston rings under load 10 N

3.3.2 Effect of precursor on wear rate

The wear rate of samples is observed to have an inverse relation with the increase of hydrogen flow rate in synthesis process till 600 sccm for both carbon precursors. The piston ring has shown lowest wear rate for 600 OPF-based coating as compared to other samples. This is due to presence of high quality graphene in 600 OPF-based coating which was earlier confirmed by Raman spectroscopy results shown in Fig. 8. While as for 800 sccm samples the wear rate has increased from 600 sccm samples, This could be due to more intensity of defects present in the coating surface as compare to the 600 sccm sample.

3.3.3 Effect of load on wear rate

The wear rate of 600 OPF-based graphene coated piston ring subjected to varying loads is given by Fig. 15. It can be observed that with the increase in load the wear rate increases within same comp coating surface. It is pertinent to mention here that there is a line contact between counter face and the specimen, and hence the contact surface is subjected to very high stresses [51].

Due to these high contact pressures (upto 5 MPa), material removal rate is subsequently increased with the slight increment in load.

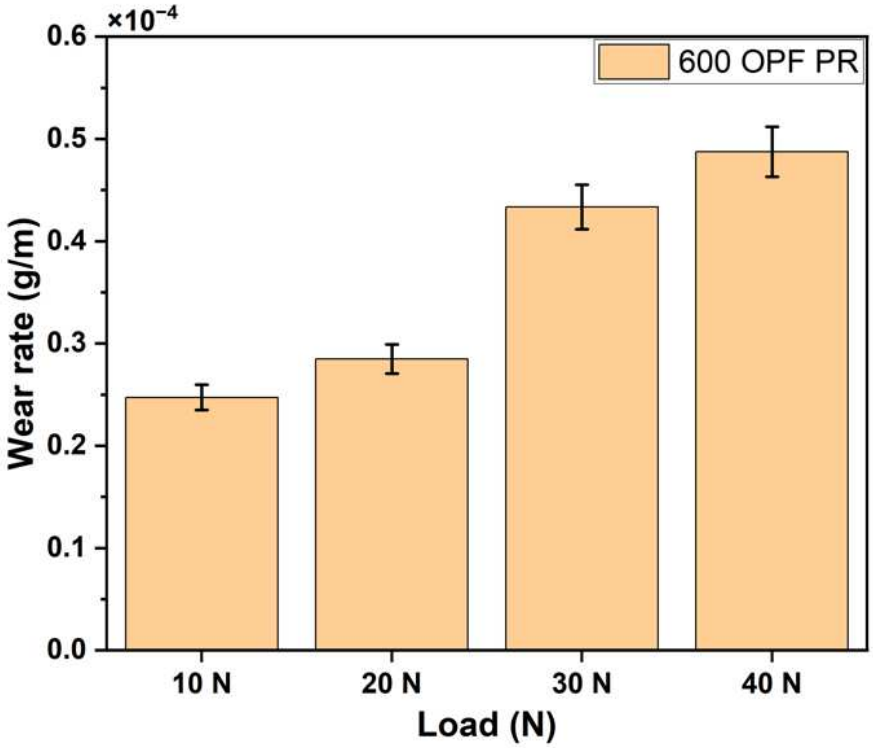

Fig. 15: Wear rate of 600 OPF piston ring subjected to varying loads

Moreover, at low loads it is expected that penetration of the asperities is less as compared to that at high loads. More penetration of asperities result in increased surface contact area, thus increased wear rate. The results obtained are in line with the Archard's law, as the wear rate is directly influenced by applied load [52]. The wear rate from 20N to 30N has shown a steep rise for 600 OPF-based graphene coated piston ring. At high loads (30N and 40N), there was less increase in the wear rate of the samples as compared to the wear rate at low loads. It is thus inferred from the above-mentioned data that the coated samples are subjected to less wear rate while undergoing transition at high loads.

3.4 Surface morphology of worn surfaces

The wear mechanism of worn 600 OPF-based graphene coated piston rings subjected to varying loads have been analysed using SEM imaging and EDX mapping. Fig. 16-19, shows the SEM images and EDX mapping of 600 OPF-based graphene coated piston ring surfaces post tribological test subjected to load 10, 20 30 and 40N respectively against stainless steel counterbody.

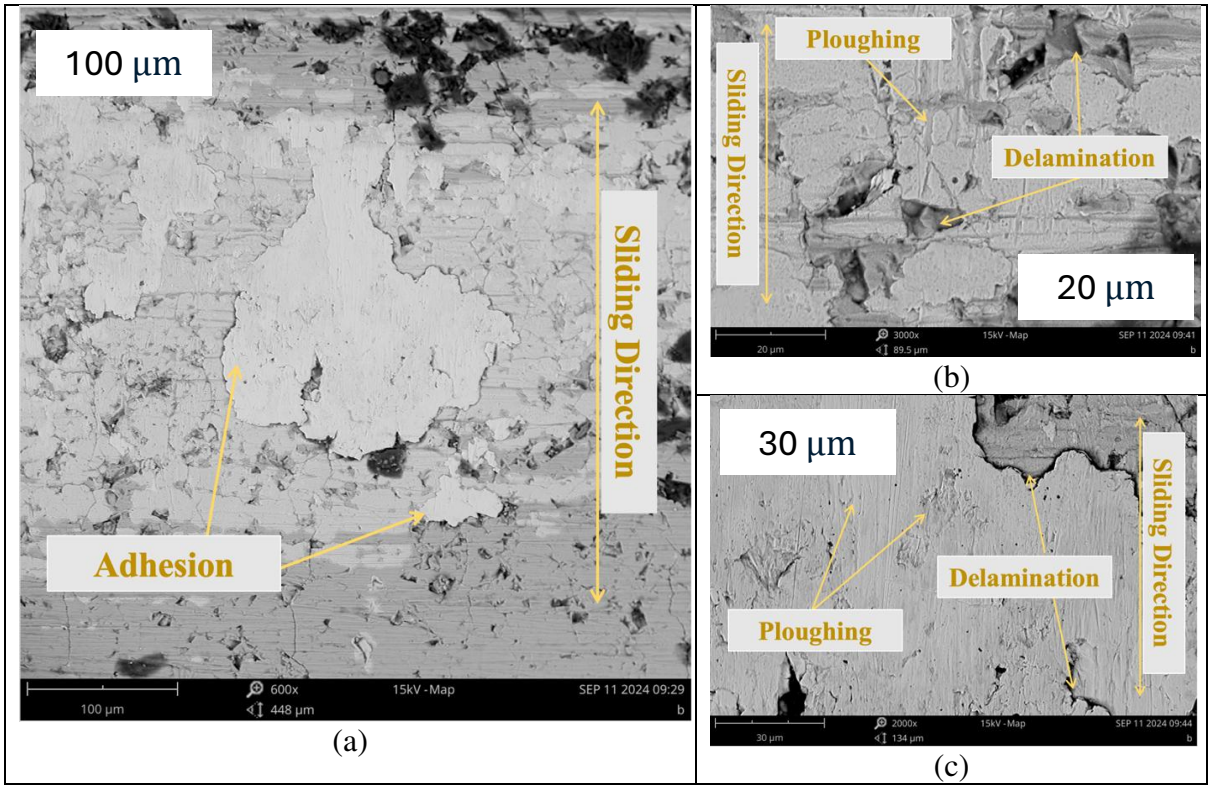

380 Fig. 16: SEM images of wear tracks of 600 OPF piston ring under load 10 N at (a) 600x
381 magnification, (b) 3000x magnification and (c) 2000x magnification

382

383

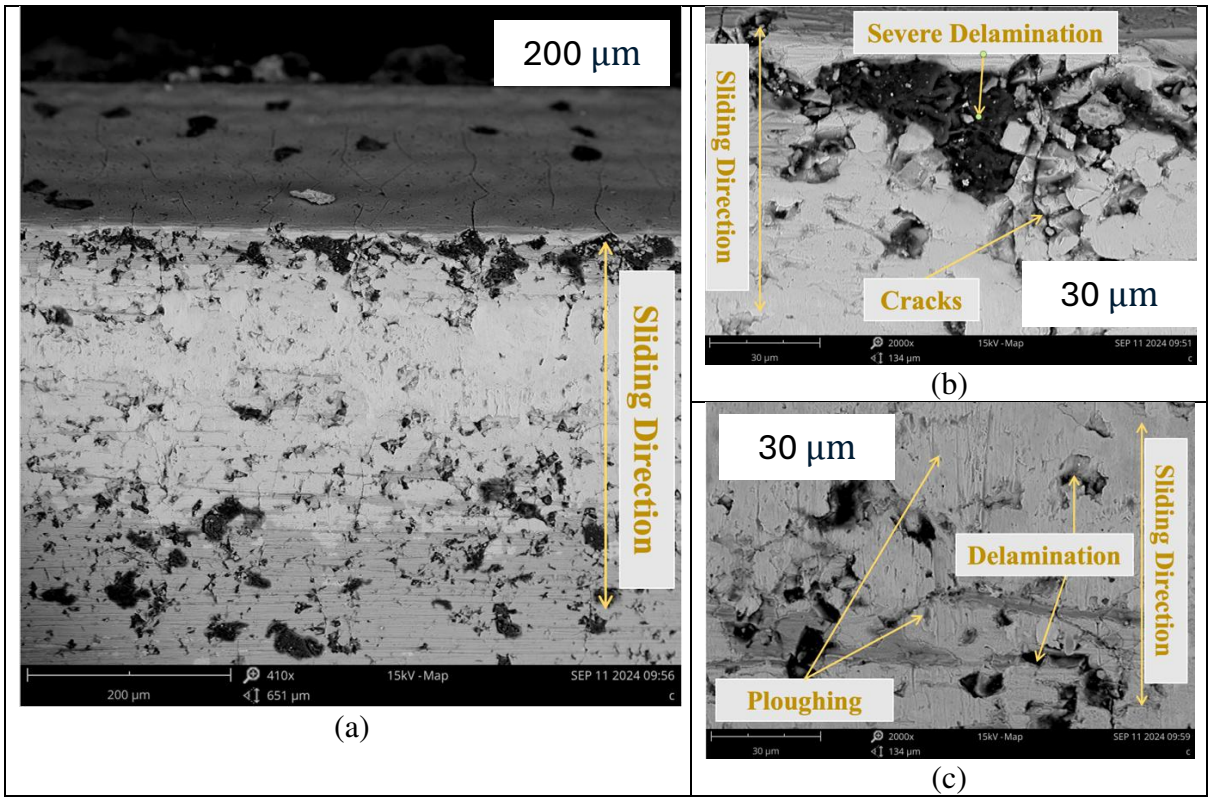

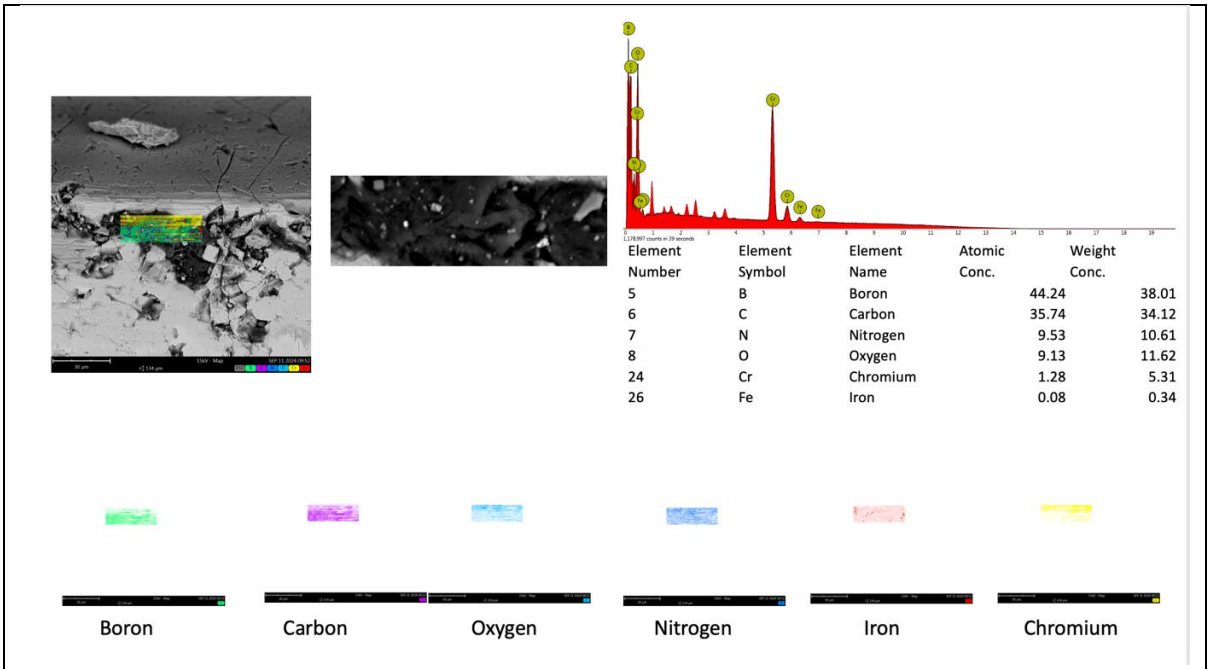

(d)

Fig. 17: SEM images (a) 410x magnification (b) Delamination spot, (c) 2000x magnification and (d) EDS Mapping of delamination spot on wear tracks of 600 OPF piston ring under load 20 N

It can be observed from Fig. 16 (a), that huge adhesion on coated surface has taken place during the wear test for 600 OPF coating under load 10N. A severe delamination is observed in Fig. 17 (b) at 3000x magnification level which is attributed to presence of some defects in graphene coating surface. In Fig.16 (c), ploughing can also be observed, which can be due to some abrasion by hard elements like chromium present on the surface of stainless steel Counterbody. Fewer microcracks can be seen in all figures on the surface of coated piston rings.

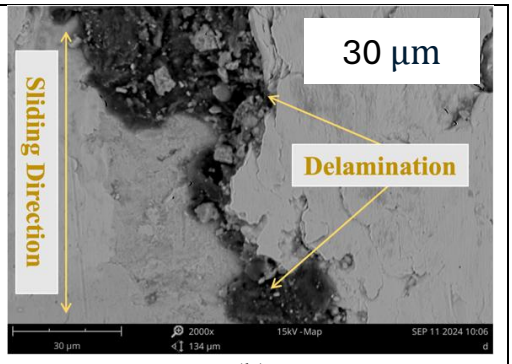

(b)

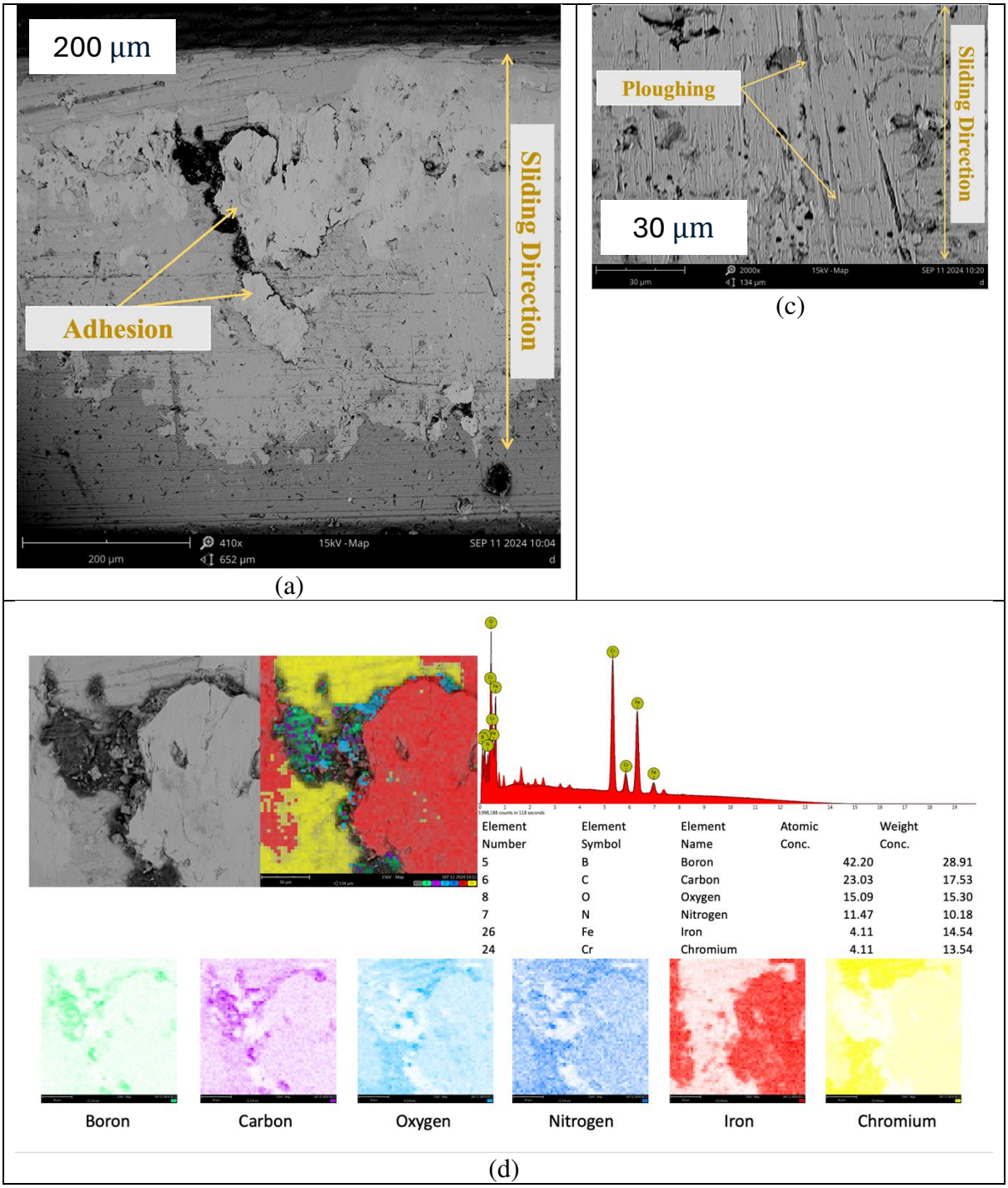

Fig. 18: SEM images (a) 410x magnification (b) Delamination spot, (c) 2000x magnification and (d) EDS Mapping of delamination spot on wear tracks of 600 OPF piston ring under load 30 N

From Fig. 17 (a), it can be observed that the surface of the 600OPF-based graphene coated piston ring surface has gone under severe delamination at multiple spots during 20N load tribological test. Fig. 17 (b), shows that some cracks in the coating surface has led to delamination of coating. EDX mapping was used to determine the elemental analysis of the delaminated point and is shown in Fig. 17(d).

It can be observed from EDX mapping Fig.17 (d), that carbon element is prominent in the delaminated area, thus it can be concluded that the coated layer is removed during the tribological test but few layers are still left over the piston ring surface. Ploughing can also be seen in Fig. 17 (c), which could be attributed to abrasive nature of removed coating particles during the test.

Similarly, from Fig. 18 (a), it can observed that the surface of coating has undergone prominent adhesion and severe delamination during the tribological test under load 30N. From Fig. 18 (c), we can observe that ploughing is seen to be significant, which is again attributed to the third body abrasion occurring during the tribological test.

From the Fig. 18 (d), EDX mapping of delaminated and adhesion spot, It is clear that Iron (Fe), has got onto the surface of piston ring and caused a huge adhesion spot. This iron could be from the stainless steel counter body which might have got transferred during the tribological test.

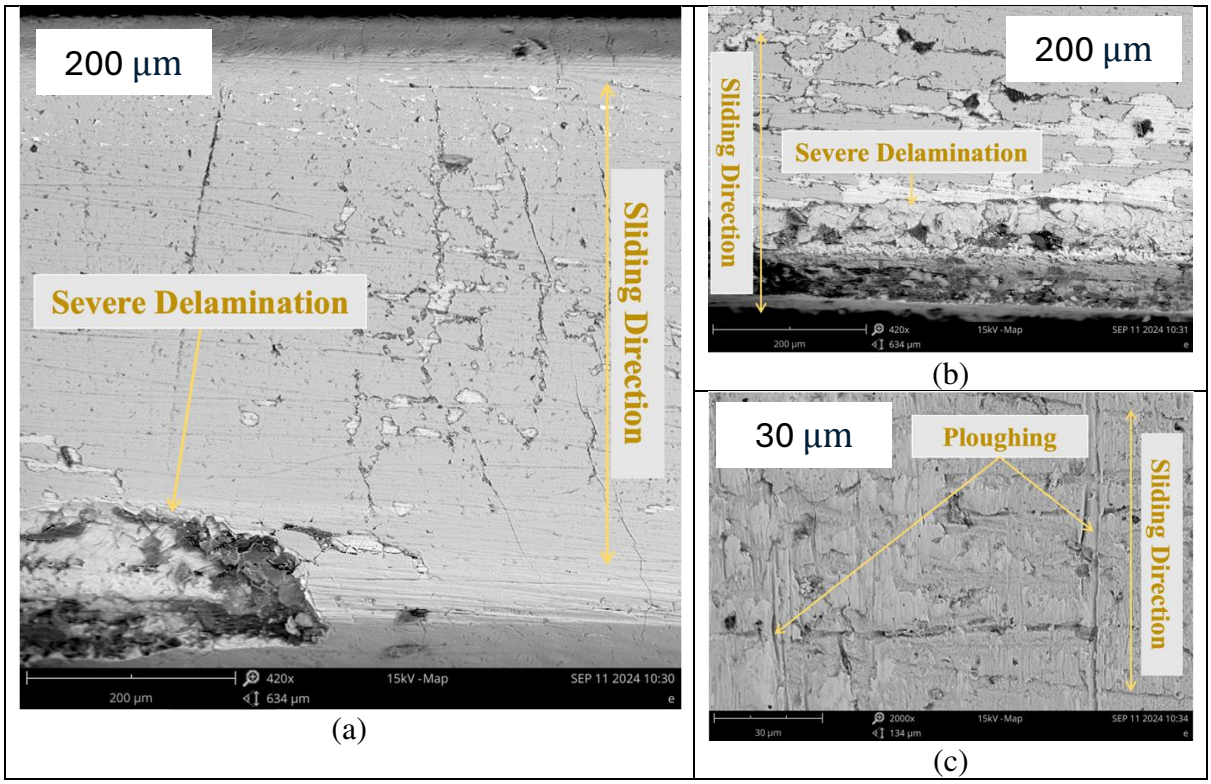

Fig. 19: SEM images of wear tracks of 600 OPF piston ring under load 40 N at (a) 420x magnification, (b) Delamination spot (c) 2000x magnification

The SEM images from Fig. 19 (a-c), show that the coating layer got severely delaminated during the tribo test at 40 N, leaving a mark on coated piston ring surface. But in COF discussion section, from Fig. 9, we observed that the COF for 600 OPF-based graphene coated piston ring got reduced, this could be due to transfer of some graphene layers to the counter

body and hence reducing friction. Also from raman spectroscopy result in Fig. 11 it was observed that the intensity of graphene oxide is much higher in 600 OPF coated sample subjected to load 40 N. This justifies the trend of COF reduction for load 40 N.

3.5 Counterbody wear rate

The wear rate for counterbodies was measured by 3D-Optical microscopy using White light interferometry. The results from white light interferometery are shown in Fig. 20 (a-l).

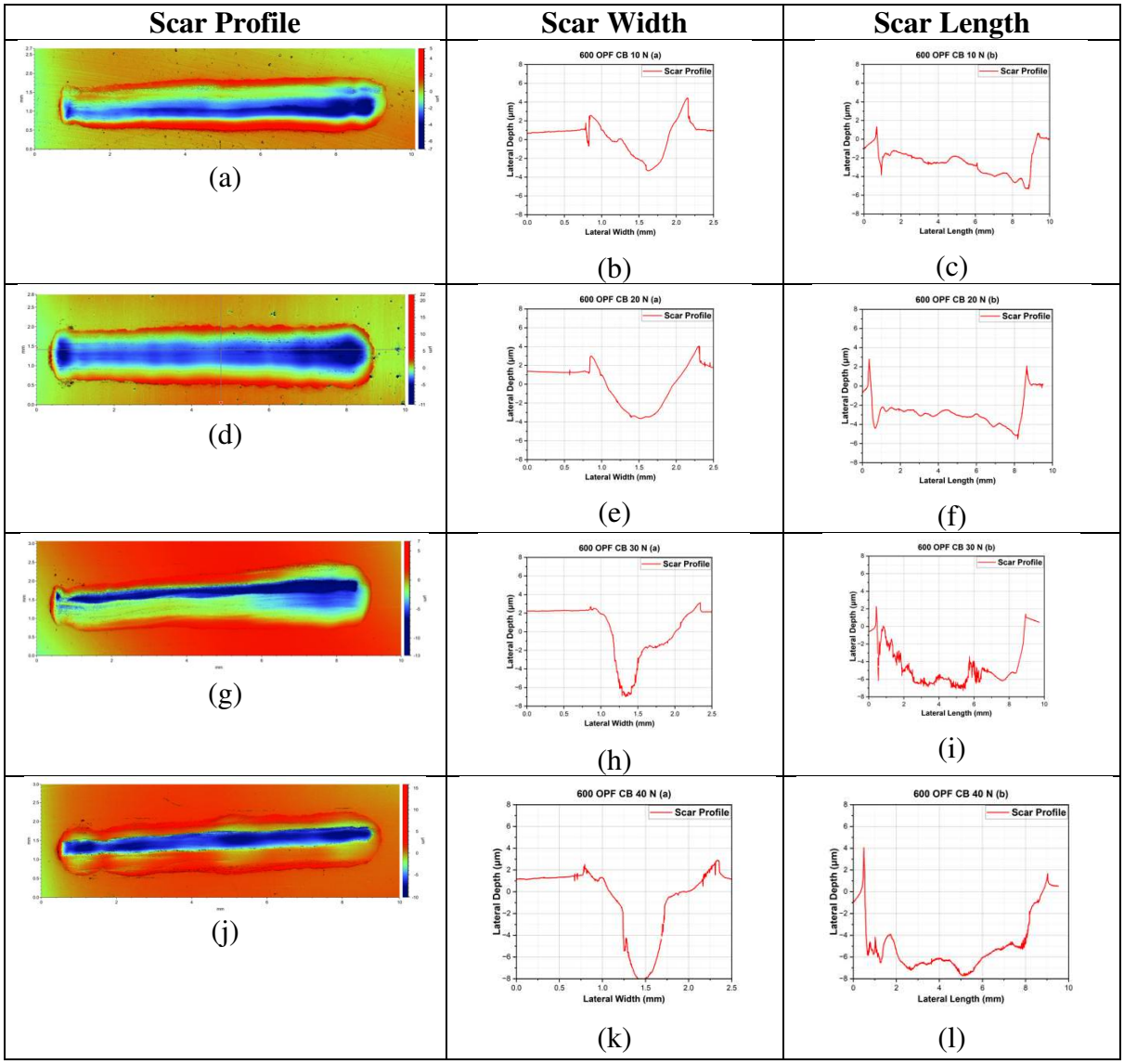

Fig. 20: Wear scar profile of counter bodies against 600 OPF piston ring (a) Scar profile for load 10N, (b) Scar width for load 10N (c) Scar length for load 10N, (d) Scar profile for load 20N, (e) Scar width for load 20N (f) Scar length for load 20N, (g) Scar profile for load 30N, (h) Scar width for load 30N (i) Scar length for load 30N, (j) Scar profile for load 40N, (k) Scar width for load 40N (l) Scar length for load 40N respectively

From Fig. 20 (h) and Fig. 20 (k), it can be observed that the depth of wear scar has increased with increase in load for counterbody which could be attributed to third body abrasion from the coating material that was removed during the tribological test at loads 30 and 40 N.

The wear rate of counter body was calculated using the results from Fig. 20, by calculating the volume loss. The wear rate for stainless steel counter body against 600 OPF-based graphene piston ring under varying loads is shown in Fig. 21.

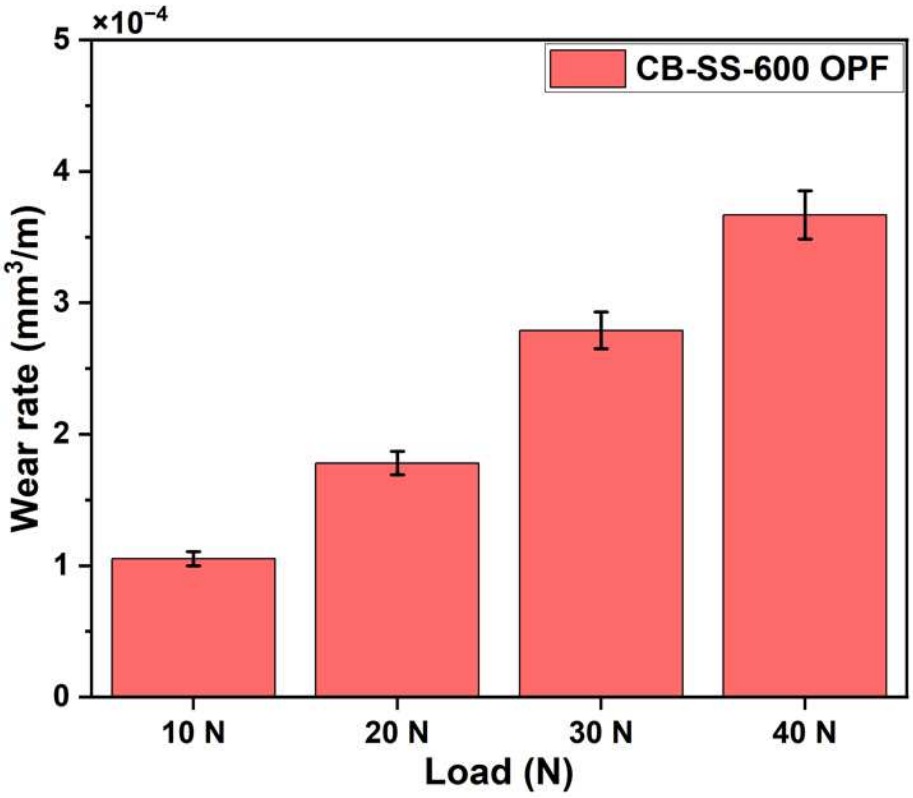

Fig. 21: Wear rate of counter bodies subjected to varying loads against 600 OPF-based graphene coated piston rings.

From Fig. 21, it is observed that with increase in load the wear rate of stainless steel surface increases against graphene coated piston rings, which is again in line with Archard's Law[51].

4. Conclusion

Graphene coatings were successfully developed on piston rings using CVD with oil palm fiber and polystyrene as carbon precursors. The key findings are:

- Oil palm fiber produced a high-quality graphene oxide coating with minimal thickness (~10 µm) compared to polystyrene.
- A 600 sccm hydrogen flow rate yielded the least defective graphene oxide layer for oil palm fiber, while 800 sccm was optimal for polystyrene-based coatings.
- Graphene-coated piston rings significantly reduced friction compared to uncoated samples, with 600 sccm oil palm fiber-based coatings showing the best tribological performance at 10 N load.
- Raman analysis confirmed the presence of graphene oxide, benefiting lubrication due to its hydrophilic nature.
- Wear rates of graphene-coated piston rings were lower than those of uncoated samples.
- The variation in COF with hydrogen flow rate highlights the need for further study, particularly for 600 and 800 sccm polystyrene-based coatings.
- Observed delamination suggests that adhesion characteristics influence the tribological behavior of the coatings. While no direct adhesion test was conducted, the wear morphology analysis provides qualitative insights. Future work should incorporate adhesion testing to better understand coating-substrate interaction.
- Further investigations on the effects of temperature and alternative counterbody materials like cast iron are recommended to enhance the applicability of graphene coatings in real-world engine conditions.

Credit authorship contribution statement

Raied Mehtab: Conceptualization, Methodology, Investigation, Formal analysis, Writing original draft. **N.W.M. Zulkifli, M. F. M. Sabri & A. Morina:** Validation, Writing – review & editing, Supervision, Data curation and formal analysis. **M. F. Abdollah, Hilmi Bin Amiruddin, S. Samion & M. F. Saharudin:** Supervision, Resources.

Acknowledgements

The authors, Raied Mehtab and Dr. Nurin Wahidah Binti Mohd Zulkifli thank the Ministry of Higher Education Malaysia for its financial assistance (under the Grant number: PT(BPKI)1000/016/018/25 Jld. 4.), to perform this experimental work. We would also like to

acknowledge the support and efforts of Dr. Ardian Morina and his team at University of Leeds for their assistance in conducting some of the tests related to this work.

Declaration of competing interest

The authors state that none of their known financial conflicts or interpersonal connections could have influenced the work that was published in this paper.

Declaration of Generative AI and AI-assisted technologies in the writing process

In order to paraphrase as well as modify sentence structures while keeping the original meaning, the authors employed Quillbolt AI and ChatGPT during the development of this work. Following their use of this tool/service, the authors took full responsibility for the publication's content and reviewed and amended it as necessary.

[1] K. Holmberg, A. Erdemir, Influence of tribology on global energy consumption, costs and emissions, Friction 5 (2017) 263–284. https://doi.org/10.1007/s40544-017-0183-5.

[2] Q.M. Mehran, M.A. Fazal, A.R. Bushroa, S. Rubaiee, A Critical Review on Physical Vapor Deposition Coatings Applied on Different Engine Components, Critical Reviews in Solid State and Materials Sciences 43 (2018) 158–175. https://doi.org/10.1080/10408436.2017.1320648.

[3] A. Gangopadhyay, A Review of Automotive Engine Friction Reduction Opportunities Through Technologies Related to Tribology, Transactions of the Indian Institute of Metals 70 (2017) 527–535. https://doi.org/10.1007/s12666-016-1001-x.

[4] R. Ferreira, J. Martins, Ó. Carvalho, L. Sobral, S. Carvalho, F. Silva, Tribological solutions for engine piston ring surfaces: an overview on the materials and manufacturing, Materials and Manufacturing Processes 35 (2020) 498–520. https://doi.org/10.1080/10426914.2019.1692352.

[5] R. Ferreira, R. Almeida, Ó. Carvalho, L. Sobral, S. Carvalho, F. Silva, Influence of a DLC coating topography in the piston ring/cylinder liner tribological performance, J Manuf Process 66 (2021) 483–493. https://doi.org/10.1016/j.jmapro.2021.04.044.

[6] C. Muratore, A.A. Voevodin, Chameleon Coatings: Adaptive Surfaces to Reduce Friction and Wear in Extreme Environments, Annu Rev Mater Res 39 (2009) 297–324. https://doi.org/10.1146/annurev-matsci-082908-145259.

[7] T.W. Scharf, S. V. Prasad, Solid lubricants: a review, J Mater Sci 48 (2013) 511–531. https://doi.org/10.1007/s10853-012-7038-2.

[8] Z. Tang, S. Li, A review of recent developments of friction modifiers for liquid lubricants (2007–present), Curr Opin Solid State Mater Sci 18 (2014) 119–139. https://doi.org/10.1016/j.cossms.2014.02.002.

[9] V.W. Wong, S.C. Tung, Overview of automotive engine friction and reduction trends–Effects of surface, material, and lubricant-additive technologies, Friction 4 (2016) 1–28. https://doi.org/10.1007/s40544-016-0107-9.

[10] A. Dehghanghadikolaei, B. Mohammadian, N. Namdari, B. Fotovvati, Abrasive Machining Techniques for Biomedical Device Applications, Journal Material Science 1 (2018) 1. https://doi.org/10.19080/JOJMS.2018.04.555654.

[11] G.A. Howarth, The synthesis of a legislation compliant corrosion protection paint system, based on waterborne epoxy, urethane and oxazolidine technology, Doctoral Dissertation, Imperial College London, 1997.
[12] O.S.I. Fayomi, I.G. Akande, O.P. Abioye, O.B. Fakehinde, New Trend in Thin Film Composite Coating Deposition: A Mini Review, Procedia Manuf 35 (2019) 1007–1012. https://doi.org/10.1016/j.promfg.2019.06.049.
[13] J.-F. Yang, Y. Jiang, J. Hardell, B. Prakash, Q.-F. Fang, Influence of service temperature on tribological characteristics of self-lubricant coatings: A review, Front Mater Sci 7 (2013) 28–39. https://doi.org/10.1007/s11706-013-0190-z.
[14] K.S. Tan, J.A. Wharton, R.J.K. Wood, Solid particle erosion–corrosion behaviour of a novel HVOF nickel aluminium bronze coating for marine applications—correlation between mass loss and electrochemical measurements, Wear 258 (2005) 629–640. https://doi.org/10.1016/j.wear.2004.02.019.
[15] H. Torres, M. Rodríguez Ripoll, B. Prakash, Tribological behaviour of self-lubricating materials at high temperatures, International Materials Reviews 63 (2018) 309–340. https://doi.org/10.1080/09506608.2017.1410944.
[16] S.M. Aouadi, B. Luster, P. Kohli, C. Muratore, A.A. Voevodin, Progress in the development of adaptive nitride-based coatings for high temperature tribological applications, Surf Coat Technol 204 (2009) 962–968. https://doi.org/10.1016/j.surfcoat.2009.04.010.
[17] Y. Wang, X.-B. Liu, Y.-F. Liu, Y.-S. Luo, Y. Meng, Microstructure and tribological performance of Ni60-based composite coatings on Ti6Al4V alloy with different Ti3SiC2 ceramic additions by laser cladding, Ceram Int 46 (2020) 28996–29010. https://doi.org/10.1016/j.ceramint.2020.08.071.
[18] J. Chen, W. Zhao, Simple method for preparing nanometer thick Ti3C2TX sheets towards highly efficient lubrication and wear resistance, Tribol Int 153 (2021) 106598. https://doi.org/10.1016/j.triboint.2020.106598.
[19] Ö. Güler, N. Bağcı, A short review on mechanical properties of graphene reinforced metal matrix composites, Journal of Materials Research and Technology 9 (2020) 6808–6833. https://doi.org/10.1016/j.jmrt.2020.01.077.
[20] K.S. Novoselov, A.K. Geim, S. V. Morozov, D. Jiang, Y. Zhang, S. V. Dubonos, I. V. Grigorieva, A.A. Firsov, Electric Field Effect in Atomically Thin Carbon Films, Science (1979) 306 (2004) 666–669. https://doi.org/10.1126/science.1102896.
[21] L. Xu, T.-B. Ma, Y.-Z. Hu, H. Wang, Vanishing stick–slip friction in few-layer graphenes: the thickness effect, Nanotechnology 22 (2011) 285708. https://doi.org/10.1088/0957-4484/22/28/285708.
[22] N.A. Mat Tahir, M.F. Bin Abdollah, N. Tamaldin, H. Amiruddin, M.R. Bin Mohamad Zin, S. Liza, Tribological performance of the graphene synthesized from fruit cover plastic waste and oil palm fiber using a CVD method, Industrial Lubrication and Tribology 72 (2020) 771–777. https://doi.org/10.1108/ILT-11-2019-0486.
[23] N.A. Mat Tahir, M.F.B. Abdollah, N. Tamaldin, H. Amiruddin, M.R.B. Mohamad Zin, Graphene coatings technology on tribology perspective., International Journal of Recent Technology and Engineering 8 (2019) 33–37.
[24] P. Kumar, M.F. Wani, Synthesis and tribological properties of graphene: A review, Jurnal Tribologi 13 (2017) 36–71.
[25] D. Berman, A. Erdemir, A. V. Sumant, Graphene: a new emerging lubricant, Materials Today 17 (2014) 31–42. https://doi.org/10.1016/j.mattod.2013.12.003.
[26] Z.B. Acunaş Karagöz, S. Demirtaş, H. Kaleli, L. Yüksek, E. Çıtak, Review of tribological behavior of graphene coatings on piston rings in engines, Industrial

574 Lubrication and Tribology 72 (2019) 243–254. https://doi.org/10.1108/ILT-06-2018-
575 0233.
576 [27] M. Son, M.-H. Ham, Low-temperature synthesis of graphene by chemical vapor
577 deposition and its applications, FlatChem 5 (2017) 40–49.
578 https://doi.org/10.1016/j.flatc.2017.07.002.
579 [28] J. Gussmagg, M. Pusterhofer, F. Summer, F. Grün, Experimental visualization of the
580 wear and scuffing evolution of a flake graphite cast iron cylinder liner, Wear 526–527
581 (2023) 204948. https://doi.org/10.1016/j.wear.2023.204948.
582 [29] M. Pusterhofer, F. Summer, D. Wuketich, F. Grün, Development of a Model Test
583 System for a Piston Ring/Cylinder Liner-Contact with Focus on Near-to-Application
584 Seizure Behaviour, Lubricants 7 (2019) 104.
585 https://doi.org/10.3390/lubricants7120104.
586 [30] F. Zhu, J. Xu, X. Han, Y. Shen, M. Jin, Tribological performance of three surface-
587 modified piston rings matched with chromium-plated cylinder liner, Industrial
588 Lubrication and Tribology 69 (2017) 276–281. https://doi.org/10.1108/ILT-11-2015-
589 0164.
590 [31] S. Stankovich, D.A. Dikin, G.H.B. Dommett, K.M. Kohlhaas, E.J. Zimney, E.A.
591 Stach, R.D. Piner, S.T. Nguyen, R.S. Ruoff, Graphene-based composite materials,
592 Nature 442 (2006) 282–286. https://doi.org/10.1038/nature04969.
593 [32] M.D. Stoller, S. Park, Y. Zhu, J. An, R.S. Ruoff, Graphene-Based Ultracapacitors,
594 Nano Lett 8 (2008) 3498–3502. https://doi.org/10.1021/nl802558y.
595 [33] L. Schlapbach, A. Züttel, Hydrogen-storage materials for mobile applications, Nature
596 414 (2001) 353–358. https://doi.org/10.1038/35104634.
597 [34] Y. Hernandez, V. Nicolosi, M. Lotya, F.M. Blighe, Z. Sun, S. De, I.T. McGovern, B.
598 Holland, M. Byrne, Y.K. Gun'Ko, J.J. Boland, P. Niraj, G. Duesberg, S.
599 Krishnamurthy, R. Goodhue, J. Hutchison, V. Scardaci, A.C. Ferrari, J.N. Coleman,
600 High-yield production of graphene by liquid-phase exfoliation of graphite, Nat
601 Nanotechnol 3 (2008) 563–568. https://doi.org/10.1038/nnano.2008.215.
602 [35] S. Stankovich, D.A. Dikin, R.D. Piner, K.A. Kohlhaas, A. Kleinhammes, Y. Jia, Y.
603 Wu, S.T. Nguyen, R.S. Ruoff, Synthesis of graphene-based nanosheets via chemical
604 reduction of exfoliated graphite oxide, Carbon N Y 45 (2007) 1558–1565.
605 https://doi.org/10.1016/j.carbon.2007.02.034.
606 [36] A. Reina, X. Jia, J. Ho, D. Nezich, H. Son, V. Bulovic, M.S. Dresselhaus, J. Kong,
607 Large Area, Few-Layer Graphene Films on Arbitrary Substrates by Chemical Vapor
608 Deposition, Nano Lett 9 (2009) 30–35. https://doi.org/10.1021/nl801827v.
609 [37] X. Li, W. Cai, J. An, S. Kim, J. Nah, D. Yang, R. Piner, A. Velamakanni, I. Jung, E.
610 Tutuc, S.K. Banerjee, L. Colombo, R.S. Ruoff, Large-Area Synthesis of High-Quality
611 and Uniform Graphene Films on Copper Foils, Science (1979) 324 (2009) 1312–1314.
612 https://doi.org/10.1126/science.1171245.
613 [38] K.S. Kim, Y. Zhao, H. Jang, S.Y. Lee, J.M. Kim, K.S. Kim, J.-H. Ahn, P. Kim, J.-Y.
614 Choi, B.H. Hong, Large-scale pattern growth of graphene films for stretchable
615 transparent electrodes, Nature 457 (2009) 706–710.
616 https://doi.org/10.1038/nature07719.
617 [39] M.J. Salifairus, S.B. Abd Hamid, T. Soga, S. A.H. Alrokayan, H. A. Khan, M. Rusop,
618 Structural and optical properties of graphene from green carbon source via thermal
619 chemical vapor deposition, J Mater Res 31 (2016) 1947–1956.
620 https://doi.org/10.1557/jmr.2016.200.
621 [40] S.M. Shinde, E. Kano, G. Kalita, M. Takeguchi, A. Hashimoto, M. Tanemura, Grain
622 structures of nitrogen-doped graphene synthesized by solid source-based chemical

vapor deposition, Carbon N Y 96 (2016) 448–453. https://doi.org/10.1016/j.carbon.2015.09.086.
[41] J.G. Kim, W.S. Kim, Y.H. Kim, C.H. Lim, D.J. Choi, Formation of graphene on SiC by chemical vapor deposition with liquid sources, Surf Coat Technol 231 (2013) 189–192. https://doi.org/10.1016/j.surfcoat.2012.06.066.
[42] H. Ji, Y. Hao, Y. Ren, M. Charlton, W.H. Lee, Q. Wu, H. Li, Y. Zhu, Y. Wu, R. Piner, R.S. Ruoff, Graphene Growth Using a Solid Carbon Feedstock and Hydrogen, ACS Nano 5 (2011) 7656–7661. https://doi.org/10.1021/nn202802x.
[43] G. Ruan, Z. Sun, Z. Peng, J.M. Tour, Growth of Graphene from Food, Insects, and Waste, ACS Nano 5 (2011) 7601–7607. https://doi.org/10.1021/nn202625c.
[44] M. Gulzar, M.H. Hassan, Tribological Study of Nanoparticles Enriched Bio-Based Lubricants for Engine Piston Ring–Cylinder Interaction, 2017. http://ezproxy.um.edu.my:2048/login?url=https://www.proquest.com/dissertations-theses/tribological-study-nanoparticles-enriched-bio/docview/2848766761/se-2?accountid=28930.
[45] A.Z. Syahir, N.W.M. Zulkifli, H.H. Masjuki, M.A. Kalam, M.H. Harith, M.N.A.M. Yusoff, Z.M. Zulfattah, M. Jamshaid, Tribological Improvement Using Ionic Liquids as Additives in Synthetic and Bio-Based Lubricants for Steel–Steel Contacts, Tribology Transactions 63 (2020) 235–250. https://doi.org/10.1080/10402004.2019.1679934.
[46] M. Sudan Reddy Dandu, K. Nanthagopal, Tribological aspects of biofuels – A review, Fuel 258 (2019) 116066. https://doi.org/10.1016/j.fuel.2019.116066.
[47] S. Arumugam, G. Sriram, Effect of Bio-Lubricant and Biodiesel-Contaminated Lubricant on Tribological Behavior of Cylinder Liner–Piston Ring Combination, Tribology Transactions 55 (2012) 438–445. https://doi.org/10.1080/10402004.2012.667517.
[48] W. Zhai, X. Shi, M. Wang, Z. Xu, J. Yao, S. Song, Y. Wang, Grain refinement: A mechanism for graphene nanoplatelets to reduce friction and wear of Ni3Al matrix self-lubricating composites, Wear 310 (2014) 33–40. https://doi.org/10.1016/j.wear.2013.12.014.
[49] S. Wan, D. Li, G. Zhang, Anh.K. Tieu, B. Zhang, Comparison of the scuffing behaviour and wear resistance of candidate engineered coatings for automotive piston rings, Tribol Int 106 (2017) 10–22. https://doi.org/10.1016/j.triboint.2016.10.026.
[50] B. Xu, Z. Zhu, S. Ma, W. Zhang, W. Liu, Sliding wear behavior of Fe–Al and Fe–Al/WC coatings prepared by high velocity arc spraying, Wear 257 (2004) 1089–1095. https://doi.org/10.1016/j.wear.2004.05.012.
[51] H. Hertz, On the contact of elastic solids, J. Reine Und Anges. Math. 92 (1881) 156–171.
[52] A. Zmitrowicz, Wear patterns and laws of wear–a review., Journal of Theoretical and Applied Mechanics 44 (2006) 219–253.